Université Kasdi Merbah Ouargla
Faculté des Mathématiques et Des Sciences de la Matière
Département de Physique

Thèse présentée en vue de l'obtention du diplôme de Doctorat LMD

Domaine: Sciences de la Matière

Filière: Physique

Spécialité: Rayonnement et Spectroscopie et Matière

Présenté par: Soumaia ABBAS

Thème

Détermination Spectroscopique des Grandeurs Optoélectroniques du SnO_2 Dopé Elaboré par Spray Ultrasonique

Soutenu Publiquement Le : 18/05/2016

Devant le jury:

Pr.	Fethi KHELFAOUI	Pr	Univ. Ouargla	Président
Pr.	Boubaker BEN HAOUA	Pr	Univ. El-Oued	Encadreur
Pr.	Kamel Eddine AIADI	Pr	Univ. Ouargla	Examinateur
Pr.	Smail CHIHI	Pr	Univ. Ouargla	Examinateur
Pr.	Saad RAHMANE	Pr	Univ. Biskra	Examinateur

Année Universitaire: 2015/2016

I dedicate this work to…

All those who participated from near or far

in the orientation of my life and my mind.

Especially, to my father,

to my mother,

to my husband,

to my sisters and brothers,

And

to all my teachers during my studies,

and all my friends.

Soumaia ABBAS

Abstract:

In this work, undoped tin dioxide (SnO_2) and fluorine doped tin dioxide (SnO_2: F) films were elaborated with spray ultrasonic technique. $SnCl_2$ and NH_4F were used as sources of SnO_2 and fluorine doping respectively. The films were deposited on 480°C heated glass. Effects of fluorine doping and films thickness on the optical, structural and opto-electrical properties of undoped and fluorine doped SnO_2: F (FTO) thin films were investigated. X-ray diffraction (XRD) patterns showed that both SnO_2 and SnO_2: F films were polycrystalline with tetragonal rutile structure. The preferential orientation for SnO_2 was along (211) plane whereas SnO_2: F preferential orientations were along (200) planes. The calculated crystallite sizes were in the average 11.57–28.16 nm. Optical transmittance spectra of the films showed high transparency of about 73-87% in visible region. The optical gap, for SnO_2 and SnO_2: F films, was found to be in the range 3.62-3.93 eV. Plasma frequencies of the films were found to be in the range 1.317×10^{15}-1.395×10^{15} Hz leading to estimated optical carrier concentration in the range of 1.575×10^{21}-$1.767\times10^{21}$$cm^{-3}$.The electrical study reveals that the films have n-type electrical conductivity and depend upon fluorine concentration. The electrical carrier concentration was found to be in the range 2.04×10^{19}–0.04×10^{19} cm^{-3} which was lower than the optically estimated one. Calculated figure of merit for FTO thin films revealed maximum value about 13.04×10^{-3} (Ω^{-1}) at λ=700 nm at fluorine concentration 6 *wt.* % for 440 nm thickness. FTIR spectra confirmed the formation of SnO_2, after fluorine doping a new vibration mode of Sn-F was appeared around 710 cm^{-1}. Contact angle on the FTO films surfaces was measured which was in the range of 66-109°. CA measured values reveals that the films surfaces have hydrophobicity properties. The elaborated FTO thin films are promising to be used as window layer in solar cells and as self cleaning materials.

Keywords: TCO thin films; SnO_2; FTO; Spray ultrasonic; Opto-electrical.

Résumé:

Dans ce travail, couches minces de dioxyde d'étain non dopé (SnO_2) et dopé par fluor (SnO_2: F) ont été élaborés avec la technique de spray ultrasons. $SnCl_2$ et NH_4F ont été utilisés comme sources de SnO_2 et de dopage au fluor, respectivement. Les couches ont été déposés sur verre chauffé à 480 °C. Effets de dopage par fluor et d'épaisseur des couches sur les propriétés optiques, structurelles et opto-électriques de couches minces SnO_2 non dopé et dopé fluor: F (FTO) ont été étudiés. Diffraction des rayons X (XRD) montrent que tous les deux motifs de SnO_2 et SnO_2: F sont des couches polycristallins avec une structure rutile tétragonale. L'orientation préférentielle pour SnO_2 était long (211) plane alors que l'orientations préférentielles de SnO_2: F étaient long (200) plans. Les tailles de cristallites calculées étaient dans la moyenne de 11.57–28.16 nm. Les spectres de transmission optique des couches ont montré une transparence élevée d'environ 73-87% dans la région visible. Le gap optique, pour SnO_2 et SnO_2: F films, a été jugée dans la gamme de 3.62-3.93 eV. Fréquences de plasma des couches ont été trouvés pour être dans la gamme 1.317×10^{15}-1.395×10^{15} Hz conduisant à la concentration de porteurs optique estimée dans la gamme de 1.575×10^{21}-$1.767\times10^{21}cm^{-3}$. L'étude électrique révèle que les films ont conductivité électrique de type n et dépendent de la concentration de fluor. La concentration de porteurs électrique a été jugée dans la gamme de 2.04×10^{19}–0.04×10^{19} cm^{-3}, qui était inférieure à celle estimée optiquement. Facteur de mérite pour FTO couches minces a révélé valeur maximale environ 13.04×10^{-3} (Ω^{-1}) à λ = 700 nm à une concentration de fluor 6 *wt*. % pour 440 nm d'épaisseur. Spectres FTIR a confirmé la formation de SnO_2, après le fluor dopage un nouveau mode de Sn-F vibration est apparu autour de 710 cm^{-1}. Angle de contact sur les surfaces des FTO couches a été mesurée qui était dans la gamme de 66-109°. CA valeurs mesurées révèle que les surfaces des films ont des propriétés d'hydrophobie. Les FTO couches minces élaborés sont prometteurs pour être utilisé comme des fenêtres dans les cellules solaires et comme matériaux auto-nettoyants.

Mots-clés: Couches minces TCO; SnO_2; FTO; Spray ultrasons; Opto-électrique.

الملخص:

في هذا العمل, تم تحضير شرائح رقيقة من ثنائي أكسيد القصدير (SnO_2) غير المطعمة و المطعمة بالفليور (SnO_2: F) بواسطة تقنية الرش فوق الصوتي. تم استعمال $SnCl_2$ و NH_4F كمصدرين للأكسيد القصدير و التطعيم بالفليور على الترتيب. الشرائح الرقيقة رسبت على ركائز من الزجاج المسخن بدرجة حرارة 480°C. في هذا العمل تم دراسة تأثير كل من التطعيم و السمك على الخصائص الضوئية, البنوية و الكهروضوئية للشرائح المحضرة. من خلال طيف حيود الأشعة السينية (XRD) تم تحديد البنية البلورية للأفلام المحضرة حيث كانت جميع العيينات ذات بنية رباعية الأقطار و متعددة البلورات. نمو الأفلام غير المطعمة كان وفق الاتجاه المفضل (211) أما الأفلام المطعمة بالفليور فكان نموها وفق الاتجاه المفضل (200). أما قيم حجم البلورات للعيينات المحضرة كانت من رتبة 11.57-28.16 nm. طيف النفاذية الضوئية للعينات المحضرة أظهر شفافية عالية للضوء المرئي قدرت بنفاذية: 73-87%. أما قيم الفجوة الطاقية الضوئية لشرائح ثنائي أكسيد القصدير غير المطعمة و المطعمة بالفليور قدرت بـ: 3.62-3.93 eV. تركيز الحوامل الحرة المحسوب من تردد البلازما كان مابين 1.575×10^{21}-$1.767\times10^{21}cm^{-3}$. ان دراسة الخصائص الكهربائية للعينات المحضرة بينت أن جميع الأفلام هي أنصاف نواقل من النوع n و قيم تركيز الحوامل الحرة المحسوبة من الدراسة الكهربائية تقدر في مابين cm^{-3} 2.04×10^{19}-0.04×10^{19} حيث يظهر أنها اقل من القيم المحسوبة بواسطة تردد البلازما. من الدراسة الكهروضوئية تم تحديد قيم معامل الجودة للعيينات المحضرة في هذا العمل فقدرت القيمة العظمى له بـ (Ω^{-1}) 13.04×10^{-3} عند λ=700 nm في العينة المطعمة بالفليور بنسبة 6 *wt.* % ذات السمك 440 nm. أما طيف الأشعة تحت الحمراء FTIR أكد تشكل بلورة ثنائي أكسيد القصدير SnO_2 , بالنسبة للعينات المطعمة بالفليور أظهر الطيف نمط اهتزاز للرابطة Sn-F حول 710 cm^{-1}. بالنسبة لتصرف هذه السطوح تجاه الماء فقد اظهر قياس زاوية التماس C لأسطح الأفلام الرقيقة المحضرة أنها كارهه للماء حيث كانت أعلى قيمة لزاوية التماس 109°. إن هذه الأفلام المحضرة في هذا العمل يمكن استعمالها في تطبيقات الخلايا الشمسية و أيضا كمواد ذاتية التنظيف.

الكلمات المفتاحية: الأفلام الرقيقة من SnO_2; FTO; TCO ; الرش فوق الصوتي; كهروضوئية.

Table of Contents

List of Figures..... **I**
List of Tables..... **III**
Nomenclature..... **IV**
Abbreviations..... **VII**
Introduction..... **12**
I. Motivation..... **12**
II. Organization of the Thesis..... **13**
References..... **14**

Chapter I: Transparent Conductive Oxides (TCOs)

I.1 TCOs Definition..... **16**
I.2 TCO Thin films..... **16**
I.3 Historical Background..... **17**
I.4 TCO's Materials..... **17**
I.5 Types of TCOs..... **18**
I.5.1 N-type TCOs..... **18**
I.5.2 P-type TCOs..... **19**
I.6 Criteria for Choosing TCOs..... **19**
I.7 Optical Properties of TCOs..... **20**
I.8 Electrical Properties of TCOs..... **22**
I.8.1 Resistance sheet (R_{sh}) and Electronic Conductivity **22**
I.8.2 Band Structure..... **22**
I.8.3 Scattering Mechanisms..... **24**
I.9 Correlation of Optical and Electrical Properties..... **25**
I.9.1 Plasma Frequency..... **25**
I.9.2 Burstein-Moss Shift..... **25**
I.9.3 Figure of Merit..... **26**
I.10 Hydrophobic Properties of TCO's Films Surfaces..... **27**
I.11 TCO's Applications..... **28**
I.11.1 Transparent Heat Reflecting Films..... **28**
I.11.2 Solar Cells..... **28**
I.11.3 Gas Sensors..... **28**
I.11.4 Other Applications..... **28**
I.12 SnO_2 Crystalline Structure..... **29**
I.12.1 SnO_2 Gap..... **29**
I.12.2 Different Phases of Tin Oxide..... **30**
I.13 Fluorine Doped Tin Oxide (FTO) **30**
References..... **32**

Chapter II: Deposition Processes & Characterization Techniques of TCOs Thin Films

II.1 Thin Film Definition……... **37**
II.2 Thin Films Growth Mechanism……... **37**
II.3 Preparation Techniques for Thin Film Deposition…….. **39**
II.3.1 Physical Vapor Deposition (PVD) …… **39**
II.3.1.1 Evaporation……... **39**
II.3.1.2 Pulsed Laser Deposition (PLD) ……... **40**
II.3.1.3 Sputtering…….. **41**
II.3.2 Chemical and Electrochemical Techniques……... **42**
II.3.2.1 Chemical Vapor Deposition (CVD) ……. **42**
II.3.2.2 Chemical Bath Deposition(CBD) …… **42**
II.3.2.3 Sol-Gel Deposition…… **43**
II.3.2.4 Spray Pyrolysis……. **44**
II.4 Ultrasonic Spray Method……. **45**
II.4.1 General Principle of the Spray Process…….. **46**
II.5 Characterization Methods…… **46**
II.5.1 X-Ray Diffraction……..... **46**
II.5.2 Scanning Electron Microscope SEM ……..….. **47**
II.5.3 Fourier Transform Infrared Spectroscopy (FTIR) Analysis…..…… **48**
II.5.4 Photoluminescence……..... **48**
II.5.5 Hall Effect…….. **49**
II.5.6 Four Probes Method……..……. **50**
II.5.7 Optical Characterization by Ultraviolet and Visible Spectroscopy……..…… **51**
II.5.8 Thickness Determination: Interference Method (Swanepoel Method) ……..…… **53**
References……..... **55**

Chapter III: Elaboration of SnO_2 Thin Films by Ultrasonic Spray & Obtained Results

III.1 Deposition of Undoped SnO_2 and Fluorine Doped SnO_2 Thin Films by Ultrasonic Spray…... **59**
III.1.1 Ultrasonic Spray Deposition System……..... **59**
III.1.2 Substrate……... **60**
III.1.3 Tin and Fluorine Sources……..…… **60**
III.1.4 Solutions Preparation…… **61**
III.1.5 Thin Films Deposition Steps…… **62**
III.2 Structural Analysis……..... **63**
III.2.1 Crystalline Structure..... **63**
III.2.2Texture Coefficient *TC(hkl)* …… **64**
III.2.3 Lattice Constants…….. **65**
III.2.4 Crystalline Sizes *D*……... **65**
III.2.5 Dislocation Density δ……... **66**
III.2.6 Thickness Effect on Structural Properties..... **67**
III.3 Morphological Characterization……..... **69**
III.4 Optical Analysis……..... **70**

III.4.1 Optical Transmission ……..... **70**
III.4.2 Thickness Determination…….. **71**
III.4.3 Optical Band Gap……. **72**
III.4.4 Thickness Effect on Optical Properties……..... **73**
III.4.5 Thickness Effect on Band Gap Value…….. **74**
III.4.6 Refraction Index……..... **74**
III.4.7 Growth Velocity……..... **74**
III.5 Reflectance and plasma frequency……..... **75**
III.6 Characterization by FTIR Spectroscopy.....……..... **77**
III.7 Sheet resistance and Hall Effect……..... **78**
References……..... **81**

Chapter IV: Results Discussion &Films Applications

IV.1 Photoluminescence Properties……..... **85**
IV.2 FTIR Results Discussion…… **89**
IV.3 Figure of merit……..... **89**
IV.4 Correlation between opto-electrical magnitudes……..... **92**
IV.4 .1 Electrical and plasmatic carriers……..... **92**
IV.4. 2 Electrical and FTIR measurements……..... **92**
IV.5 Applications……..... **93**
IV.5.1 Window layer for solar cells……..... **93**
IV.5.2 Self cleaning materials……... **93**
References……..... **96**
Conclusion and Perspectives……..……..…… **99**
Appendix A: The CITOTEST Super White Microscope Slides (CSW slides)…….. **102**
Appendix B: Solutions Preparation..……... **104**
Appendix C: List of Publications and Attended Conferences……..…..... **105**

List of Figures

Figure I.1:	Spectral dependence of TCOs materials: λ_g and λ_p are the wavelengths at which the band gap absorption and free electron plasma absorption take place……..	**20**
Figure I.2:	Schematic representation of the band structure of undoped (a) and doped (b) TCO in the vicinity of the top of the valence band and bottom of the conduction band. The grey areas denote the occupied states……..……..	**24**
Figure I.3:	Schematic representation the enlarging of optical gap by BM effect: (a) undoped TCO (b) doped TCO. The grey areas denote the occupied states……..	**26**
Figure I.4:	Contact angles…….	**27**
Figure I.5:	Bonding geometry of the tetragonal unit cell of SnO_2 in the rutile structure……..	**29**
Figure I.6:	SnO_2 Band structure……	**30**
Figure II.1:	Schematic diagram showing stages of thin film growth…….	**38**
Figure II.2:	Classification of Thin Film Deposition Techniques…….....	**39**
Figure II.3:	Schematic diagram of the evaporation technique…….....	**40**
Figure II.4:	Schematic diagram of the Laser ablation system…….....	**40**
Figure II.5:	Schematic diagram of the sputtering method…….....	**41**
Figure II.6:	Deferent steps of chemical vapor deposition (CVD) technique……..	**42**
Figure II.7:	Schematics of chemical bath deposition (CBD) method……	**43**
Figure II.8:	Schematics of sol-gel technique: (a) spin coating process; (b) dip coating process	**44**
Figure II.9:	Schematics of spray pyrolysis showing its various parts…….	**44**
Figure II.10:	Ultrasonic spray experimental set-up schematic…….....	**45**
Figure II.11:	Schematics of X-ray diffractometer…….....	**47**
Figure II.12:	Diagram of scanning electron microscope …….....	**48**
Figure II.13:	A Simple FTIR Spectrometer Layout ……..……...	**49**
Figure II.14:	(a) Schematic band diagrams for the photoluminescence processes and (b) the experimental set-up for PL measurement……	**50**
Figure II.15:	Hall voltage circuit…….....	**51**
Figure II.16:	Four-Point Collinear Probe Resistivity Configuration……	**52**
Figure II.17:	Schematics of UV-VIS spectrophotometer…….....	**52**
Figure II.18:	Transmittance spectrum general form of SnO_2 thin film…….	**53**
Figure II.19:	Plot of $(\alpha h\upsilon)^2$ vs. $(h\upsilon)$ ……..……...	**52**
Figure III.1:	Photo of the used ultrasonic spray deposition system…….	**59**
Figure III.2:	Microscopic glass slide used as substrate…….....	**60**

Figure III.3:	(a):Photo of the used stannous chloride ($SnCl_2$, $2H_2O$). (b):Photo of the used ammonium fluoride……..	**61**
Figure III.4:	Glass coated by F doped SnO_2 thin film…….....	**63**
Figure III.5:	XDR patterns of F (0–12 wt.%) doped SnO_2 thin films……..	**64**
Figure III.6:	Variations of grain size and dislocation density of FTO thin films as a function of F concentration…….....	**67**
Figure III.7:	XRD patterns of F-doped SnO_2 films as function of film thickness……	**67**
Figure III.8:	Grain size and dislocation density variations as function of film thickness for FTO films…….....	**69**
Figure III.9:	SEM images of SnO_2: F (3-12 wt. %): (a) 3 wt. %, (b) 6 wt. % and (c) 12 wt. %	**70**
Figure III.10:	Spectral transmittance plot of F (0–12 wt.%) doped SnO_2 thin films……	**70**
Figure III.11:	Band-gap estimation from Tauc relation of F (0–12 wt.%) doped SnO_2 films…...	**72**
Figure III.12:	Transmittance spectra of SnO_2: F at 6 wt. % thin films for different film thicknesses…….....	**73**
Figure III.13:	Band-gap estimation of SnO_2: F 6 wt. % thin films for different film thickness…	**74**
Figure III.14:	Plot of film thickness as function of deposition time for estimating growth velocity…….....	**75**
Figure III.15:	Spectral reflectance plot of F (6–12 wt. %) doped SnO_2 thin films ……..	**75**
Figure III.16:	FTIR spectra of un-doped and F-doped SnO_2 films…….....	**77**
Figure III.17:	Variations of carrier concentration and sheet resistance of FTO films with different fluorine doping…….....	**80**
Figure IV.1:	PL spectrum of undoped SnO_2 thin film prepared by ultrasonic spray……...	**85**
Figure IV.2:	PL spectra of undoped and fluorine doped SnO_2 thin films prepared by ultrasonic spray…….....	**86**
Figure IV.3:	PL spectrum of SnO_2: F 3wt. % thin film prepared by ultrasonic spray ……	**86**
Figure IV.4:	Variations of PL emission peaks area of FTO films with different fluorine concentration…….....	**87**
Figure IV.5:	Schematic diagram of band structure of undoped and F-doped SnO_2 films……	**88**
Figure IV.6:	Figure of merit of undoped and F-doped SnO_2 as a function of wavelengths…….	**90**
Figure IV.7:	Figure of merit of SnO_2: F 6 wt. % as a function of wavelengths for different film thickness…….....	**92**
Figure IV.8:	Contact angle measurements of undoped and fluorine doped SnO_2 thin films…	**94**

Abbreviations

TCO	Transparent Conductive Oxides
BC	Conduction Band
ITO	Indium Tin Oxide
FTO	Fluorine-doped Tin Oxide
AZO	Aluminum-doped Zinc Oxides
IZO	Indium -doped Zinc Oxides
GZO	Gallium-doped Zinc Oxides
ATO	Antimony Tin Oxide
TNO	Niobium-doped Anatase oxide
VB	Valence Band
NUV	Near Ultraviolet
VIS	Visible
NIR	Near Infrared
BM	Burstein-Moss
PVD	Physical vapor deposition
PLD	Pulsed laser deposition
CVD	Chemical vapor deposition
CBD	Chemical Bath Deposition
XRD	X-Ray Diffraction
JCPDS	Joint Committee Power Diffraction Standards
FTIR	Fourier Transform Infra-Red
SEM	Scanning Electron Microscope
PL	Photoluminescence
UV-VIS	Ultraviolet and Visible
rt	room temperature
wt	Weight
FWHM	full width at half-maximum
CA	Contact angle

I. Motivation

Recently, increased technical activity has been directed towards both the deposition and characterization of transparent conducting oxides (TCOs) thin films such as: tin oxide (SnO_2) [1, 2], indium oxide (In_2O_3), indium tin oxide (ITO) and titanium oxide (TiO_2) owing to the multifunctional properties that such films exhibit [3, 4]. Almost all countries have initiated programmes to develop indigenous alternate TCOs. The main objective of all technological developments is to develop TCO materials with low resistivity and high transparency. Transparent conductive oxides (TCOs) have high optical transmission at visible wavelengths and electrical conductivity close to that of metals. They, also, reflect near infrared and infrared (*i.e.*, heat) wavelengths. Consequently, TCOs are used in a wide range of applications, including solar cells [1], gas sensors [5], optoelectronic devices, flat panel displays; liquid crystal displays (LCD), electro-chromic smart windows, as well as architectural coatings [5, 6].

TCOs materials have been intensely developed since the late 1970's but have actually been around for a century [7]. Cadmium oxide (CdO) was the first TCO and was used in solar cells in the early 1900's [8]. Tin dioxide (SnO_2) belongs to the class of TCOs materials; SnO_2 is available and easy to deposit as thin films by using several techniques. The surface and materials properties of SnO_2 (and doped SnO_2) make it suitable for major TCOs applications. Tin dioxide was first deposited on glass in the 1940s for electroluminescent panels [9, 10]. Since then, applications and deposition processes have mushroomed. TCOs thin films and materials are some of the most commonly used materials that we depend on for a wide range of applications.

This work is devoted to the study of the deposition of undoped and fluorine doped SnO_2 thin films on glass substrates by ultrasonic spray process. The aim of this study is to determine spectroscopically the optoelectronic magnitudes of F doped SnO_2 prepared by ultrasonic spray. In this work, tin dichloride $SnCl_2$ is used as precursor and ammonium fluoride (NH_4F) as source of fluorine doping. The choice is based on the possibility to obtain these materials with low cost; in addition, SnO_2 is easy to deposit on glass substrate by

ultrasonic spray. The elaborated undoped and F-doped SnO_2 thin films are analyzed and different films properties (structural, optical and opto-electrical) are studied using spectroscopic methods, the results will be discussed to examine the quality of elaborated thin films and to determine the appropriate applications. In this thesis, detailed theoretical study and organization is performed in order to present a coherent view of the subject.

II. Organization of the Thesis

This thesis is organized into the following structure:

Chapter I: It starts with giving the definition of transparent conducting oxides, then introducing a historical background of TCOs. Following that, the main properties that distinguish TCOs materials and their important applications are listed. Finally, it ends up with the definition of tin oxide and FTO materials.

Chapter II: In this chapter, the concept of Thin Film is presented with explaining the different steps of thin films growth mechanism. After that, the techniques and methods used in thin films deposition are described, focusing on ultrasonic spray technique. In addition, the different analytical techniques used to characterize TCO thin films are described.

Chapter III: In this chapter, firstly, the experimental steps used to deposit undoped and F doped SnO_2 thin films prepared by ultrasonic spray are introduced. Whereas, secondly, the experimental results obtained by the analysis of the elaborated SnO_2: F thin films are presented with focusing on the structural, optical and opto-electrical properties of undoped and F doped SnO_2 thin films prepared by ultrasonic spray method.

Chapter IV: This chapter introduces a broad discussion of the experimental results obtained by the analysis of the elaborated SnO_2: F thin films, which presented in the previous chapter, with offering the appropriate applications for the elaborated films according to the obtained results.

The work is summed up with a general conclusion that summarizes the primary findings of this thesis and, in closing, suggests avenues for future studies.

Every solid object has a surface; this surface is the discontinuity in the bulk materials properties and has been the target of modifications (artistic decoration and/or functional improvement) since the earliest times of mankind. Today, modern products offer even more new functions with the unusual properties that often cannot be found in bulk sample. These product materials open completely new areas of applications. The multi-functionality of these technical products concerns their surface properties. Surface coating of glass, with different types of films, is one of the technologies that occupy a key position in the material and product development. Transparent Conducting Oxide (TCO), thin films are the most important of these materials [1].

I.1 TCOs Definition

There is a family of metal oxides, which in addition to being transparent can become conductive (n-type) if they have an excess of electrons in their lattice. This excess of electrons can be created either by structural defects inducing an imbalance in the stoichiometry of the oxide as SnO_2 [2], or by a suitable doping [3]. Such transparent conductive oxides are called (TCOs). TCOs have a high gap and are, in fact, degenerate semiconductors, *i.e.* that their Fermi level is close to the conduction band (BC) , and even within this band for TCO highly doped. This means that the BC already contains a considerable number of electrons at room temperature, owing them conducting properties. In addition, TCO with high gaps, are transparent in the region of visible light [4]. Simple definition can be given to TCOs: Transparent Conductive Oxides are degenerate semiconductors with wide band gap that have the dual property of being good electric conductors and transparent in the visible region [5]. TCO thin films in practical use as transparent electrodes are reported to exhibit conductivity of the order of 10^4 $S.cm^{-1}$ and an average transmittance above 80% in the visible range. The TCO semiconductors suitable for transparent electrodes should have a carrier concentration over than 10^{20} cm^{-3} [6].

I.2 TCO Thin films

Transparent conductive oxides (TCOs) thin films are layers of a material deposited on substrate. The term *thin films*, as used here, refers to material layers with thicknesses too small (0.1-1000nm) but having completely the bulk materials properties as described in, *e.g.* ASTM standards.

I.3 Historical Background

TCOs have been known for more than century. However, their technological and commercial use as thin films has been emerged for half a century. The history of TCO starts from 1907, with the discovery of Cadmium Oxide (CdO) thin film by a German scientist Karl Badeker [7]. Due to its small band gap, CdO transparency was too low to be used for practical applications. The first transparent conductive oxide, which has been patented for his discovery in the undoped and in the doped states, is the tin oxide SnO_2 in 1931 and 1942 respectively [8, 9]. In 1951, tin-doped indium oxide Sn-In_2O_3 which called (ITO) was synthesized by J.M. Mochel [8]. The practical use of TCO started with discovery of tin-doped In_2O_3 in 1954 by G. Rupprecht [10]; Binary compounds TCOs such as ZnO, SnO_2, In_2O_3 and their alloys were also recognized in 1960s [11]. Ternary compounds such as Cd_2SnO_4, $CdSnO_3$ and $CdIn_2O_4$ were developed as TCO materials prior to 1980. After this date, impurity-doped ZnO such as ZnO: Al and ZnO: Ga along with abundant of binary compounds were developed. In 1990s, new TCO materials consisting of multi-component oxides, like combination of ZnO, CdO, In_2O_3 and SnO_2, have been born [12]. All TCOs, mentioned above, are n-type. There was no p-type TCO reported until 1993, when H. Satu and his co-workers reported NiO as p-type TCO [13]. The second report on $CuAlO_2$ as a p-type TCO was published in 1997, by H. Kawazoe et al., with considerable improvements over NiO [14]. This opened the development of a series of p-type TCOs [15]. However, until now no efficient p-type TCO having opto-electrical properties, comparable to its n-type counterpart, is available. If there would be an efficient p-type TCO, it can be used as transparent pn-junction which will lead to a new generation of electronics known as “transparent electronics” [6].

I.4 TCO’s Materials

The first TCO was discovered when a sputter deposited cadmium thin film underwent incomplete thermal oxidation with post-deposition heating in air [16, 17]. Since this realization, many others TCOs materials have been developed with tin oxide, indium oxide, or zinc oxide as the main component which are displayed in Table I.1 [18]. Indium tin oxide (ITO) is an In_2O_3-rich compound of In_2O_3 and SnO_2 that has become the principal TCO material due to its excellent optical and electrical properties, having average resistivity of about 10^{-4} Ω·cm [16, 19]. However, alternatives to ITO are being investigated because of the high cost and scarcity of indium.

Table I.1: *Common TCO materials.*

Main Component	Dopant
Tin Oxide (SnO_2)	Fluorine (F)
	Antimony (Sb)
Indium Oxide (In_2O_3)	Tin (Sn)
	Zinc (Zn)
Zinc Oxide (ZnO)	Aluminum (Al)
	Boron (B)
	Gallium (Ga)

Fluorine-doped tin oxide (FTO) is the second most used TCO which is one of our goals in this study. Aluminum, Indium and gallium-doped zinc oxides (AZO, IZO and GZO, respectively) are also good alternatives to ITO, but they tend to degrade faster than ITO and FTO in hot, moist atmospheres [16, 20]. Antimony tin oxide (ATO) is Sb-doped tin oxide (SnO_2).Due to its low cost, ATO properties have been studied and looks to be a promising as an alternative to ITO [16]. Anatase TiO_2 doped with Nb oxide (TNO) has properties that ITO does not possess, such as high refractive index, high transmittance in the infrared region and high chemical stability in reducing atmosphere [21].

I.5 Types of TCOs

All TCOs can be classified into two major classes; the **p-type** and the **n-type**, based on their majority charge carriers. The n-type conductivity of TCOs results from Oxygen-vacancies, interstitial metal ions impurities due to some intrinsic or extrinsic defects and n-type doping ions, while the p-type conductivity is due to oxygen-excess, interstitial metal ions vacancies and p-type doping [6].

I.5.1 n-type TCOs

An n-type TCO is one in which the majority charge carriers are electrons. Most of the known TCOs are n-type and, therefore, are most commonly found in practical applications. The presence of extrinsic donors generates free electrons resulting in n-type conductivity. Historically, most research to develop TCO thin films as transparent electrodes has been conducted using n-type semiconductors [6].

I.5.2 p-type TCOs

In p-type TCOs the majority charge carriers are holes having positive charge. Preparation of p-type TCOs needs shallow acceptor level slightly above the valence band. Among these p-type TCOs reported so far, NiO is considered to be one of the most promising [14]. Advancements in p-type TCO materials development are still in a growth stage. Conductivity of p-type oxide semiconductors is lower than the n-type conductivity [22], because of the strong localization behavior of positively charged holes at the valence band edge of the oxide materials, which cannot migrate even under a consistent electric filed [6].

I.6 Criteria for Choosing TCOs

It is apparent from the diversity of applications for TCOs that no material is most suitable for all uses. Depending on which material property is of most importance, different choices are made. Table I.2 lists some of the most important criteria that may influence the choice of a TCOs materials.

Table I.2: *Choice of transparent conductive oxides [23].*

Property	Material
Highest transparency	ZnO: F, Cd_2SnO_4
Most easily etched	ZnO: F
Best resistance to H Plasmas	ZnO: F
Best thermal stability	SnO_2: F, TiN, Cd_2SnO_4
Best mechanical durability	SnO_2: F, TiN
Best chemical durability	SnO_2: F
Lowest cost	SnO_2: F
Least toxic	SnO_2:F, ZnO: F
Lowest deposition temperature	In_2O_3: Sn, ZnO: B, Ag
Highest conductivity	In_2O_3: Sn
Lowest plasma frequency	SnO_2: F, ZnO: F
Highest plasma frequency	In_2O_3: Sn, Ag, TiN

For each application, the most suitable TCO is the one that shows good electrical conductivity coupled with good optical transparency [24]. The physical, chemical, and thermal durability, etchability, plasma frequency, thickness, deposition temperature, toxicity, and cost are other factors that may also influence the choice of transparent conducting material for any particular application [23].

I.7 Optical Properties of TCOs

An important feature of TCOs is the existence of a transmission window covering most part of the visible spectrum. In literature, the optical transmission is defined as the ratio between transmitted intensity averaged over all values in between 400 nm and 700 nm and incoming light intensity. The typical spectral dependence of TCOs is schematically shown in Figure I.1.

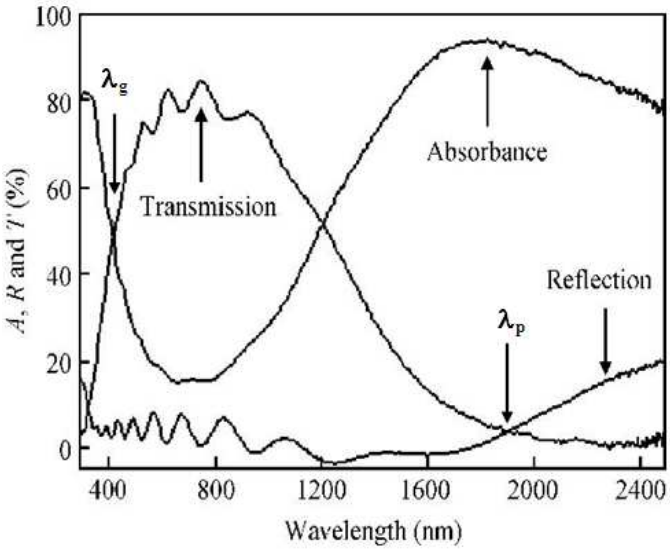

Figure I.1: *Spectral dependence of TCOs materials: λ_g and λ_p are the wavelengths at which the band gap absorption and free electron plasma absorption take place [25].*

The transmission window is defined by two regions where no light is transmitted due to different phenomena: At low wavelengths ($\lambda<\lambda_g$) the absorption due to the fundamental band gap dominating. Near-and UV energy is high enough to equal the band gap energy. This energy is absorbed and transformed to band to band transitions, and no light is transmitted. For longer wavelengths, in the (near) infrared (IR) part of the spectrum, no light is transmitted due to the plasma edge ($\lambda>\lambda_p$) where light is reflected by the material as described by the classical Drude free electron theory [26].

In the free electron model, the electrons may be considered as plasma whose density is set into motion by the electric field component of the electromagnetic field. The plasma oscillates at a natural frequency ω_p (resonance or plasma frequency). This frequency corresponds to the plasma wavelength λ_p and has orders of 1-4 μm for TCOs [23]. The plasma wavelength λ_p is expressed as follow:

$$\lambda_p = \frac{2\pi c}{\omega_p} \tag{I.1}$$

where ***c*** is light speed at vacuum. The interaction of free electrons with the electromagnetic field influences the relative permittivity ***ε*** of the material, which is expressed as a complex number:

$$\varepsilon = (n - ik)^2 \tag{I.2}$$

The real and imaginary part is the refractive index (***n***) and the extinction coefficient (***k***) respectively. These parameters determine the reflectance and absorptance of the material. Close to the plasma frequency, the properties of the material changes drastically. In the infrared (IR) part of the spectrum, below this critical value ($\omega<\omega_p$, or $\lambda>\lambda_p$) the imaginary part of Eq. I.2 is large, and the penetrating wave drops off exponentially [27]. The real part is negative, and the material has near-unity reflectance. For $\omega>\omega_p$ (or $\lambda<\lambda_p$) the imaginary part tends to zero, and absorption is small. The refractive index is positive and almost constant with frequency according to:

$$n = \varepsilon_\infty^{1/2}\sqrt{1-\left(\omega_p/\omega\right)^2} \approx \sqrt{\varepsilon_\infty} \tag{I.3}$$

Here ε_∞ is the high frequency permittivity. The TCO behaves like a dielectric and is transparent in the region for $\omega>\omega_p$ [28]. In this transparent regime the film is weakly absorbing ($k^2<<n^2$) and the transmission can be expressed as [29]:

$$T = (1-R)\exp(-\alpha t) \tag{I.4}$$

R is the zero degree incidence reflectance, t is the film thickness and α is the absorption coefficient which depends on the wavelength according to:

$$\alpha = \frac{4\pi k}{\lambda} \tag{I.5}$$

Close to λ_g the reflectance is zero and the absorption coefficient as a function of wavelength can be obtained easily from the transmission curve.

Band gap energy, for direct transition semiconductor, is calculated from the Tauc plot [30], $(\alpha h\upsilon)^2$ versus the photon energy $(h\upsilon)$. If $(\alpha h\upsilon)^2$ is extrapolated to the x-axis intersection ($\alpha^2=0$), Eq. I.6 implies that the photon energy equals the band gap energy ($h\upsilon \approx E_g$). The following relation applies for direct allowed transitions:

$$(\alpha h\upsilon)^2 = (h\upsilon - E_g) \tag{I.6}$$

where $(h\upsilon)$ is the photon energy. This method is commonplace to extract band gap energy from transmission data.

I.8 Electrical Properties of TCOs

I.8.1 Resistance sheet (R_{sh}) and Electronic Conductivity

For thin films of uniform thickness ***t***, the electrical resistance is sometimes expressed as the sheet resistance ($\boldsymbol{R_{sh}=\rho/t}$ in $\boldsymbol{\Omega/cm^2}$). Other than the thickness, the sheet resistance is independent of the film dimensions. The resistivity $\boldsymbol{\rho=t\times R_{sh}}$ is defined as the inverse of the conductivity where:

$$\rho = \frac{1}{\sigma} = \frac{1}{e.\mu.N} \tag{I.7}$$

where $\boldsymbol{\sigma}$ is the conductivity, ***N*** is the number of charge carriers in the material, $\boldsymbol{\mu}$ is their mobility and ***e*** is the elementary electron charge [31, 32].

I.8.2 Band Structure

The presence of a band gap, providing low absorption in the visible range, is an essential feature of TCOs. The top of the valence band is mostly formed by the oxygen **2*p*** bands, whereas the bottom of the conduction band is composed of a single and highly dispersed ***s*** band. The oxygen **2*p*** orbitals are low in energy, therefore, a large band gap can be obtained in metal oxides. In intrinsic stoichiometric oxides, coexistence of electrical

conductivity besides visible transparency is not possible. However, substitutional doping by cationic donors or anion vacancies can create charge carriers, *i.e.* electrons. The donor (or acceptor) states alter the electronic band structure of the material. For increased donor density, the donor states merge with the conduction band at a certain critical density N_c, whose magnitude can be estimated by Mott's criterion [31, 32].

$$N_c^{1/3}.a_0^* \approx 0.25 \tag{I.8}$$

The effective Bohr radius a_0* is given by:

$$a_0^* = \frac{h^2 \varepsilon_0 \varepsilon_r}{\pi e^2 m_c^*} \tag{I.9}$$

Where ε is the static dielectric constant of the host lattice and m_c* is the effective mass of the electrons in the conduction band. The critical density N_c is calculated as 6.4 x10^{18} cm^{-3} for In_2O_3. In general, the carrier density in TCOs is by far larger than this (up to 10^{21} cm^{-3} in ITO). Above this N_c (Mott critical density), free electrons behaviors can be expected. The donor states have merged with the conduction band leading to degenerating material. The Fermi energy E_F is determined by the highest occupied state of the conduction band, and one can write:

$$E_F = \frac{\hbar^2 k^2}{2m_c^*} = \frac{\hbar^2}{2m_c^*}(3\pi N_v)^{2/3} \tag{I.10}$$

Figure I.2 represents a schematic TCO band structure. The later is approximated by parabolic functions of k close to the band edges. The valence band maximum and conduction band minimum are both located at k=0, in the case of direct band gap material [33].

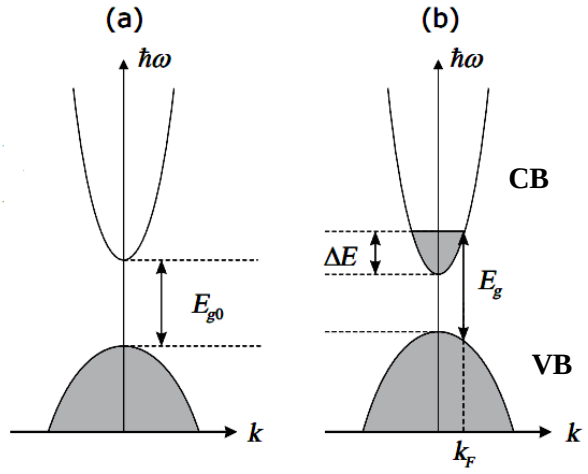

Figure I.2: *Schematic representation of the band structure of undoped (a) and doped (b) TCO in the vicinity of valence band top and conduction band. The grey areas denote the occupied states.*

I.8.3 Scattering Mechanisms

As mentioned previously, the conductivity of TCOs is reflected from the mobility that can be expressed as:

$$\mu = \frac{e.\tau}{m^*} = \frac{e.l}{m^*.V_F} \tag{I.11}$$

Where $\boldsymbol{\tau}$ is the relaxation time, V_F is the drift velocity, $\boldsymbol{l}$ is the mean free path of the charge carriers and m^* is the electron effective mass. The parameters are affected by the different scattering mechanisms: lattice scattering, ionized impurity scattering, neutral impurity scattering, electron-electron scattering, electron-impurity scattering and grain boundary scattering [34]. The total mobility, μ_{tot}, can be written as function of above sited mobilities μ_i:

$$\frac{1}{\mu_{tot}} = \sum_i \frac{1}{\mu_i} \tag{I.12}$$

In crystalline TCOs, all scattering mechanisms have little effect except the ionized impurity scattering [35]. However, TCOs deposited at lower temperatures have lower crystalline nature, and high doping concentrations result in the formation of neutral complexes [36]. In these cases, grain boundary and neutral impurity scattering should also be taken into consideration. We will return to such mechanisms in the result discussion.

I.9 Correlation of Optical and Electrical Properties

I.9.1 Plasma Frequency

The optical parameters of TCOs such as plasma frequency and refractive index are affected by the electrical properties of the material. Plasma frequency is the frequency of periodic oscillations of charge density in conducting media. The earlier mentioned plasma resonance frequency is not a fixed value, but varies with the electron concentration [6]. If the frequency incident light is higher than the plasma frequency of the material, the free charges cannot respond to the incident light and the material behaves as a transparent dielectric. However, in contrast case, materials reflect and absorb incident light. For most TCOs materials, the plasma frequency falls in the near-infrared region, that is why, the TCOs show good transparency to the visible light [23]. The plasma frequency is proportional to the square root of the conduction electron concentration (see Eq. I.13). Thus, larger value of doping concentration increases the plasma frequency thereby reducing the wavelength range of transparency while increasing the electrical conductivity and vice versa [6]. The relationship between plasma frequency and carrier concentration is expressed by:

$$\omega_p = \sqrt{\frac{Ne^2}{\varepsilon_0 \varepsilon_\infty m_c^*}} \tag{I.13}$$

where N is the carriers concentration, e is the electronic charge, ε_0 is the permittivity of free space, ε_∞ is the high frequency permittivity and m^* is the effective mass. At this frequency, the dielectric-like visible transmittance equals the metallic-like IR reflectance (T=R). Thus, the IR reflectivity of the material can be tuned, which is important for heat reflecting or low emissive window applications [37, 38].

I.9.2 Burstein-Moss Shift

For heavily doped TCOs, a gradual shift of the band gap towards higher energy as the electron density increases is generally observed [34]. This well known effect is attributed to the Burstein-Moss shift (BM shift) [39]. In heavily doped TCOs, the lowest states in the conduction band are blocked. Hence transition can only take place to energies above E_F (see Figure I.3), enlarging the effective optical gap(case generally confronted in experimental estimation of optical band gap as it will be discussed in results chapter). The energy gap

between the top of valence band and lowest empty state in the conduction band (both assumed parabolic) can be given by:

$$E_g = E_g^0 + \Delta E_g^{BM} - \hbar\Sigma \tag{I.14}$$

in this formula $E_g^{\,0}$ is the intrinsic band gap and the BM shift given by:

$$\Delta E_g^{BM} = \frac{\hbar^2}{2m_{vc}^*}(3\pi^2 n)^{2/3} \tag{I.15}$$

here m_{vc}* is the reduced effective mass of the electron carriers given by:

$$\frac{1}{m_{vc}^*} = \frac{1}{m_c^*} + \frac{1}{m_v^*} \tag{I.16}$$

where m_c* and m_v* are effective mass of the carriers in the conduction and valence band respectively. The term $(\hbar\Sigma)$ in Eq. I.14 represents self energies due to electron-electron and electron-impurity scattering (generally neglected), causing a band gap narrowing that counteracts the BM shift. This effect is of importance at very high carrier concentrations (order 10^{21} cm^{-3}).

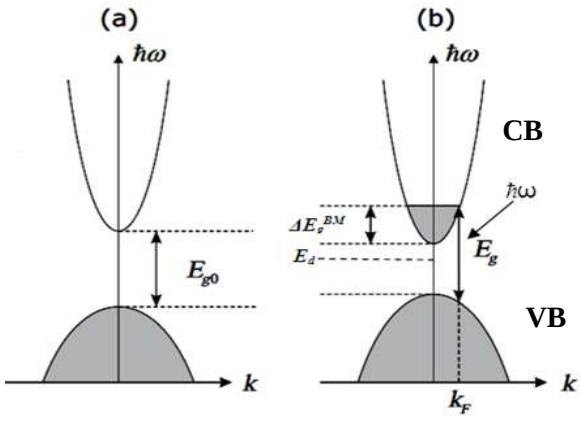

Figure I.3: *Schematic representation the enlarging of optical gap by BM effect: (a) undoped TCO (b) doped TCO. The grey areas denote the occupied states.*

I.9.3 Figure of Merit

Effective TCOs should possess both high electrical conductivity and low absorption of visible light. Thus, the ratio between the transmittance (T) and sheet resistance (R_{sh}) of transparent conducting films is called figure of merit (φ) for rating these materials. Later,

Haacke defined a more suitable measure as for some applications optical absorption is too low at maximum φ [40]. This new figure of merit is defined as:

$$\varphi = \frac{T^{10}}{R_{sh}} \tag{I.17}$$

This magnitude finds its application in solar cells [41].

I.10 Hydrophobic Properties of TCO's Films Surfaces

Water drops on hydrophilic, or water-loving surfaces spreads across it to maximize the contact area. For a hydrophobic surface, drops of water sit up high to minimize their area of contact with the material. A hydrophilic surface has a contact angle (where the droplet's surface meets the material) less than 30 degrees; whereas a hydrophobic surface has a contact angle greater than 90 degrees as shown in Figure I.4.

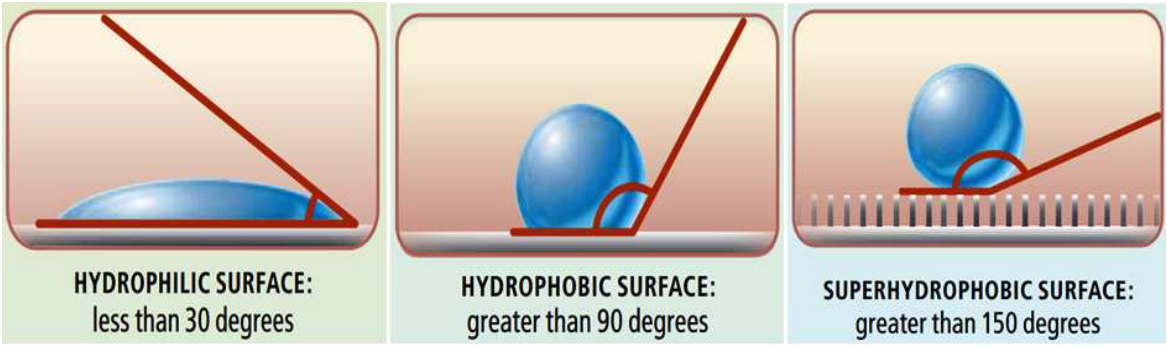

Figure I.4: *Contact angles for hydrophilic, hydrophobic and superhydrophobic surfaces.*

The basic law determining the equilibrium shape of a liquid drop on a surface was formulated by Thomas Young. The drop's shape is governed by the action of forces pulling at the three phase contact line of the drop in the plane of the solid, which is where the solid/liquid, liquid/gas and solid/gas interfaces meet. The forces (per unit length) acting at this line are the surface tensions, and their balance yields the famous equation bearing Young's name:

$$\gamma_{sg} - \gamma_{sl} = \gamma_{lg} \cos\theta_Y \tag{I.18}$$

Where θ_Y is Young angle, γ_{sg}, γ_{sl} and γ_{lg} are the surface tensions between the three phases solid/gas, solid/liquid, and liquid/gas respectively. If the drop is small enough such that

gravity is negligible, which typically is the case for drops of millimetre size down to micrometres, the drop will have the shape of a spherical cap and the liquid/gas interface meets the solid surface at an angle θ_Y, which is called the intrinsic contact angle of the drop [42, 43].

I.11 TCO's Applications

I.11.1 Transparent Heat Reflecting Films

TCOs films, on one hand, efficiently reflect infrared heat radiation; on the other hand, they transmit light effectively in the visible region as if they were insulators. Such spectrally selective films have wide applications in solar thermal energy conversion, solar photovoltaic conversion, solar heating, window insulation and thermal insulation in lamps. Their ability to reflect thermal infrared heat is exploited to minimize the heating cost in winter and air-conditioning cost in summer [6, 44].

I.11.2 Solar Cells

TCOs films permit the transmission of solar radiation directly, with little or no attenuation, to the active region. In addition, TCOs films can serve simultaneously both as a low-resistance contact to the junction and anti-reflection coating of the active region. Solar cells utilizing these transparent conducting coatings are now being fabricated widely [41, 44].

I.11.3 Gas Sensors

The semiconducting properties of the TCOs films have been exploited in sensing of various gases [44]. Many TCOs are suitable for detecting combustible, reducing, or oxidizing gases such as: CO, CO_2, H_2, H_2O, H_2S, NH_3, CH_4, SO_x and NO_x. For instance, all the following oxides (SnO_2, ZnO, In_2O_3, WO_3 and TiO_2) show a gas response in their conductivity. However, the most commonly used gas sensing materials are SnO_2 and ZnO [45-48].

I.11.4 Other Applications

In addition to these above main applications, TCOs films are now being widely used in a variety of other applications such as:

- Microwaves' windows are coated with TCO which allows visible light to pass and block microwaves so as to protect eyes [23].
- The electrical conductivity of TCOs is exploited in flat panel displays [23].
- Electric current is passed through TCOs to defrost windows of vehicles and to keep the deep cases of freezers frost-free [23].
- TCOs can also be formed into invisible security circuits on windows and transparent radio antennas built into automobile windows [23].
- TCOs can be used as photocatalytics, where active surfaces can cause breakdown of organic molecules adsorbed on these surfaces under the action of solar irradiation. Thus, unpleasant pollutants can be decomposed into tasteless, odorless, or at least less toxic compounds [44].

I.12 SnO_2 Crystalline Structure

As it is known, tin oxide (SnO_2) is a crystal of white color, the density is 7.0096 g/cm^3, melting point is about 2000°C. The SnO_2 films have predominantly amorphous or polycrystalline structure with a tetragonal lattice of rutile with parameters a=b=4.737Å, c=3.185Å as provided from JCPDS card No: 41-1445, with two tin atoms and four oxygen atoms in the unit cell. Tin dioxide with the rutile structure (see Figure I.5) is an n-type semiconductor with a wide and direct band gap more than 3.6 eV [49, 50].

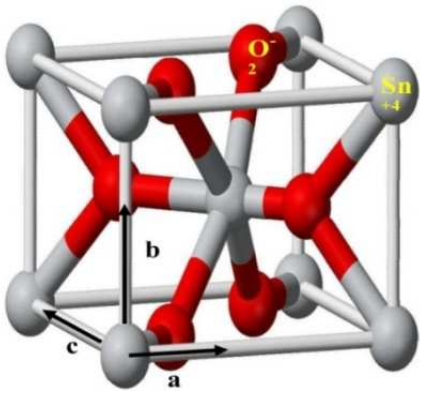

Figure I.5: *Bonding geometry of the tetragonal unit cell of SnO_2 in the rutile structure [51].*

I.12.1 SnO_2 Gap

Tin oxide thin film gap varies from 3.6 to 4.2 eV, its variations are related to the deposition techniques. The extreme of the valence band and the conduction band are on the

same axis of $\vec{k}$ vectors (Figure I.6) ($\vec{k}$ is the wave vector in the Brillouin zone center Γ) which means direct band gap. Electrons transitions from the valence band to the conduction band are vertically [5].

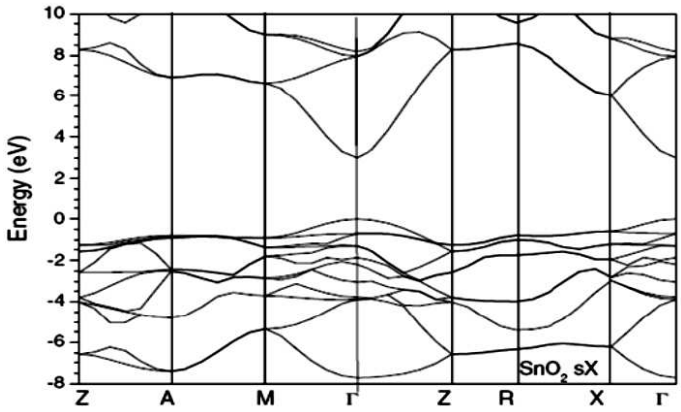

Figure I.6: *SnO_2 Band structure [51].*

I.12.2 Different Phases of Tin Oxide (SnO_2)

SnO_2 films are amorphous when they are deposited at temperatures below than 350°C. films crystallization begins only from this temperature. SnO_2 thin films produced by different deposition techniques are generally non-stoichiometric, they represent metastable phases such as SnO and Sn_3O_4. SnO phase appears at the deposition temperature of 400°C and disappears at temperature of 500°C. This phase decomposes to SnO_2 and Sn with annealing temperature of 450°C. Sn_3O_4 phase appears during heat treatment at 600°C for 5 minutes and transformed into SnO_2 after annealing at 600°C for one hour [5].

I.13 Fluorine Doped Tin Oxide (FTO)

One of the most promising TCO materials is tin oxide (SnO_2). Tin oxide is a transparent conductive oxide n-type. It was the first TCO to be marketed. SnO_2 is chemically inert material and mechanically hard; it is resistant at high temperature and stable against the atmosphere [5] and acidic solutions. Tin oxide has a free electron concentration in the range of 10^{19} to 10^{20} cm^{-3}. Electrical properties can be improved with doping. Doping with fluorine (F), antimony (Sb), cobalt (Co), Cerium (Ce), iron (Fe), palladium (Pd), niobium (Nb), molybdenum (Mo) and indium (In) has been achieved to improve tin oxide (SnO_2) properties [52-58]. Among these dopants, fluorine has been proved to be the most effective and achieved

commercial TCO due to its low cost and simplicity. When fluorine ions are introduced into the SnO_2 lattice, the fluorine ions are supposed to occupy the oxygen ions due to the following reasons: similar ionic radius (F^-:1.17Å, O^{2-}:1.22Å) [59], comparable bond energy with Sn (Sn–O bond ~527.6k.J.mol^{-1}, Sn–F bond ~466.5k.J.mol^{-1}). Thus, the lattice is nearly unable to distinguish between fluorine ions and oxygen ions [5, 60].

A survey of literatures reveals that the oxygen vacancy (V_O) and substitution of fluorine for oxygen (F^-) are the main donors in un-doped SnO_2 film and FTO film, respectively. In the substitution of oxygen by fluorine, each F^- substitutes an O^{2-} and$^-$ provides one free electron causing an increase in the carrier concentration in comparison with non doped SnO_2. However, there is a solubility limit of fluorine ions in the SnO_2 lattice, beyond which the excess fluorine ions do not occupy the proper lattice position to produce free carriers, but to fill the interstitial site. The interstitial fluorine has a negative effect on carrier concentration at high fluorine levels [61].

Conclusion

From this chapter one can conclude the following points:

- Transparent Conductive Oxides are degenerate semiconductors with wide band gap that have the dual property of being good electric conductors and transparent in the visible region.
- Historically, TCOs were limited primarily to Indium tin oxide, tin oxide with fluorine doping and zinc oxide with aluminum doping. Over the past 5–10 years the field has exploded to include a vastly increased number of n-type TCOs and new p-type TCOs.
- TCOs films are widely used in applications such as Transparent Heat Reflecting Films, Solar Cells and Gas Sensors.
- One of the most promising TCO materials is tin oxide (SnO_2). Tin oxide has a rutile structure, and it is an n-type semiconductor with a wide and direct band gap more than 3.6 eV.
- Fluorine doped tin oxide (FTO) has been proved to be the most effective and achieved commercial TCO due to its low cost and simplicity.

The principal application of TCOs is in thin films form; which can be deposited by various deposition techniques. Each of these techniques has advantages and disadvantages as it will be shown in this purpose. Chapter II outlines various techniques used for synthesizing thin films, with detailed account of spray ultrasonic method used in this work. Thin films growth mechanisms will be described in this chapter too. Also, different techniques, used to characterize structural, optical and electrical properties of elaborated SnO_2 and F-doped SnO_2 thin films, for this work, will be described with relevant principles of their operation and working.

II. 1 Thin Film Definition

Thin films are thin material layers ranging from fractions of a nanometer to several micrometers in thickness. So a thin film is defined as a low dimensional material created by condensing, one by one, atomic/molecular/ionic species of matter. The very presumes idea of a thin film is the existence of a substrate; If no substrate, it is foil [1-3].

II.2 Thin Films Growth Mechanism

There are several stages in the growth process, from the initial nucleation of the deposits to the final continuous three-dimensional film formation state. These stages, schematically illustrated in Figure II.1, will be discussed briefly in this section.

1. Nucleation

Nucleation or small cluster formation is the primary process in the deposition. In this stage, the impinging atoms may or may not uniformly cover the substrate surface in the first spurt of deposition. The atoms occupy only a fraction or specific part of the substrate surface and it deposit preferentially on certain sites leading to assemblages of atoms known as nuclei or clusters, as Figure II.1 a shows[4].

2. Island Structure

The schematic representation the island structure is illustrated in Figure II.1 b. The islands consist of comparatively larger nuclei generally of three dimensional nature, however, their height is much less than their lateral dimensions [4].

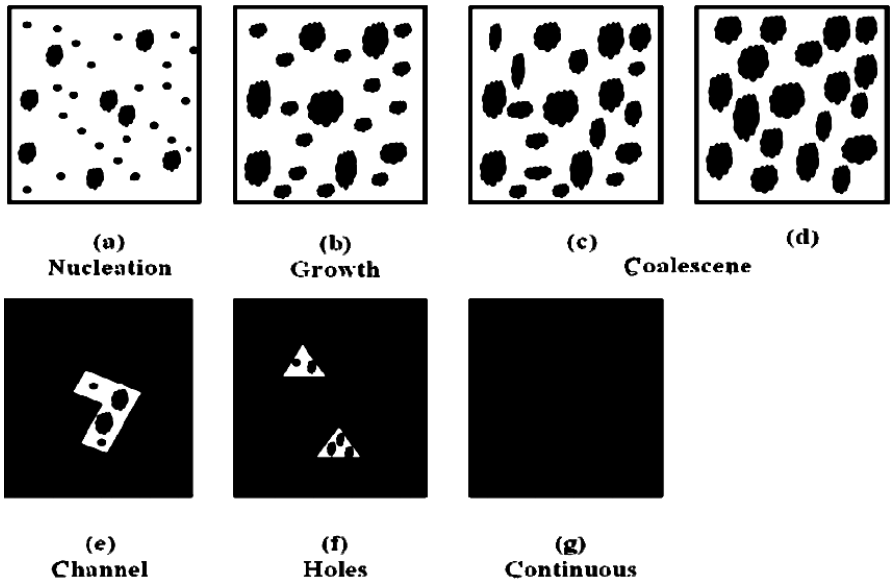

Figure II.1: *Schematic diagram showing stages of thin film growth [4].*

3. Coalescence

As islands grow, they develop some characteristic shapes. Then, with further growth, each island coalesce with the neighboring ones. Small islands disappear rapidly (Figure II.1 c and d) [4]. This process can take place amongst islands which are appropriately positioned and the coalesced islands generally become triangular or hexagonal shaped as a result of the rapid decrease of the uncovered substrate surface area followed by a slow rise of it.

4. Channel and Holes

As the coalescence continues with deposition, it will be result a network of the film with channels in between (Figure II.1 e). These channels do not remain void, but the secondary nuclei start to grow within these void spaces. With further deposition, these nuclei will increase in size along with the film thickness to formation of new islands and to join the main islands by bridging the gaps. Sometimes, even with increasing film thickness, these channels may not be completely filled up. Thus, leaving some holes or gaps in the film structure (Figure II.1 f). With further growth, these holes or gaps will decrease in size [4].

5. Continuous Film

When these gaps are completely bridged by the secondary nuclei, films will be

continuous. However, it often happens that some void space may still remain unbridged (Figure II.1 g) [4].

II.3 Preparation Techniques for Thin Film Deposition

Thin films are formed by deposition, either physical or chemical methods (see Figure II.2). The properties of thin films are extremely sensitive to the method of preparation. Physical method covers the deposition techniques which depend on the evaporation or ejection of the material from a source, whereas chemical methods depend on a specific chemical reaction [5].

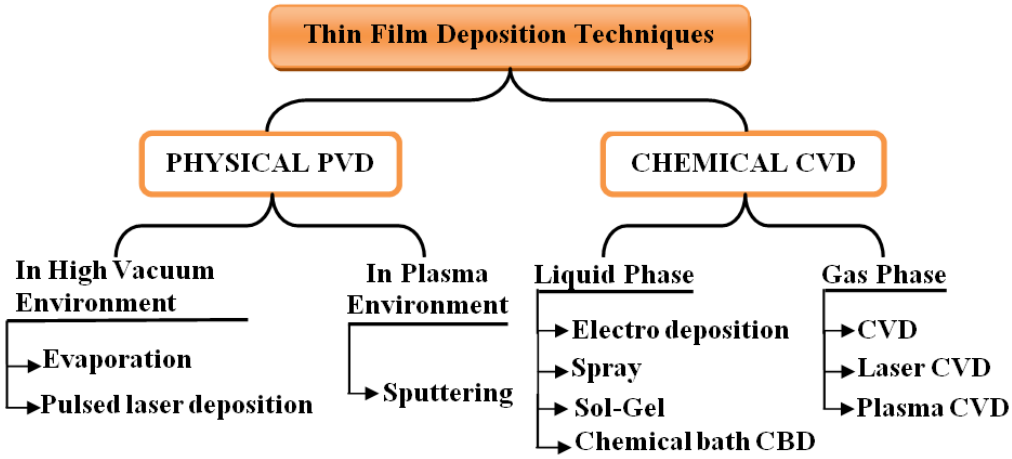

Figure II.2: *Classification of Thin Film Deposition Techniques.*

II.3.1 Physical Vapor Deposition (PVD)

PVD processes proceed along the following sequence of steps:

a) The solid material to be deposited is physically converted to vapor phase;
b) The vapor phase is transported across a region of reduced pressure from the source to the substrate;
c) The vapor condenses on the substrate to form the thin film [6, 7].

II.3.1.1 Evaporation

Evaporation techniques are widely used for the preparation of thin layers, hence, very large number of materials can be evaporated. In this technique, the source material must be

vaporized in the vacuum under high pressure. Vacuum allows vapor particles to travel directly to the target (substrate), where they are condensed to forming thin film. For evaporation process a heat source, can be resistant or any other thermal source, used to reach high temperature sufficiently to produce the desire vapor and to avoid chemical reaction between evaporant and other by products in the vapor phase [8, 9]. The basic set-up of evaporation technique is shown in Figure II.3.

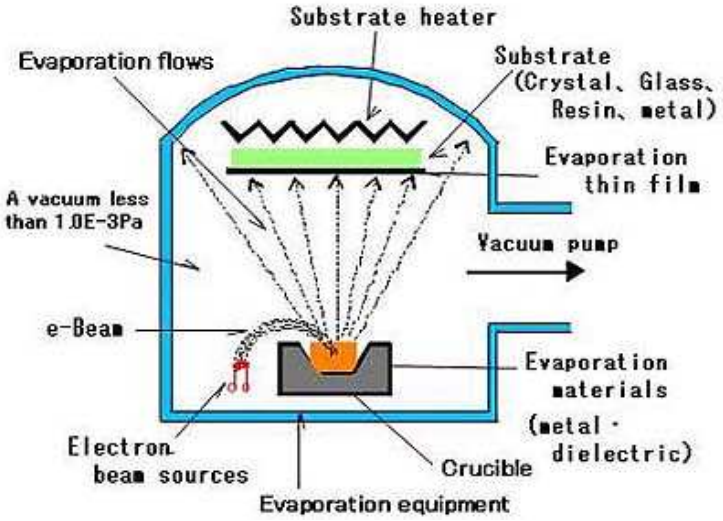

Figure II.3: *Schematic diagram of the evaporation technique.*

II.3.1.2 Pulsed Laser Deposition (PLD)

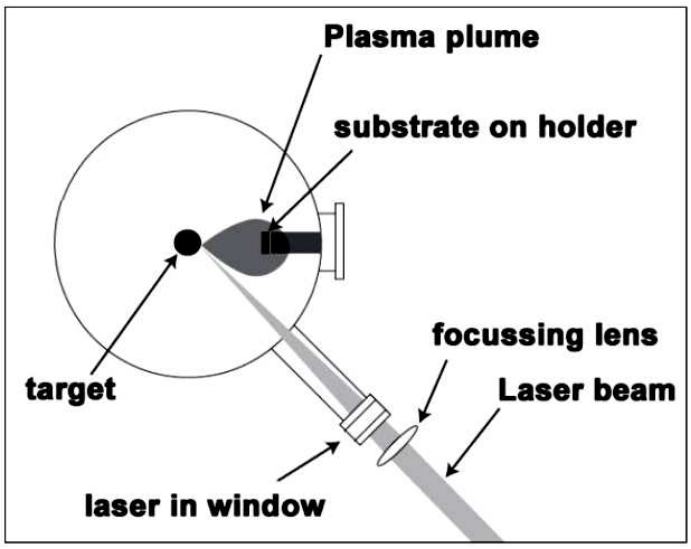

Figure II.4: *Schematic diagram of the Laser ablation system.*

Pulsed laser deposition (PLD) is a physical vapor deposition process, carried out in a vacuum system. In PLD, shown schematically in Figure II.4, a pulsed laser is focused onto a target of the material to be deposited. Pulsed laser can easily achieve the energy required for a material to transform into plasma. For sufficiently high laser energy density, each laser pulse vaporizes or ablates a small amount of the material creating a plasma plume. The ablated material is ejected from the target in a highly forward-directed plume. The ablation plume provides the material flux for film growth [10, 11].

II.3.1.3 Sputtering

If a surface of target material is bombarded with energetic particles; it is possible to cause surface atom ejection, this process is known as sputtering. The ejected atoms can be condensed on the substrate to form thin film. Typically, the substrate is placed in a vacuum chamber opposite the target (made of the coating material being sputtered). The chamber is evacuated and backfilled with a process gas (Argon), the gas is ionized with a positive charge which creates plasma. As the relatively large argon ions impact the target, atoms/molecules of target material are physically removed from it. This process is similar to the interaction of billiard balls in a confined space. Majority of sputtered atoms/molecules land on the substrate due to its close proximity [12]. Figure II.5 shows a schematic diagram of the sputtering method.

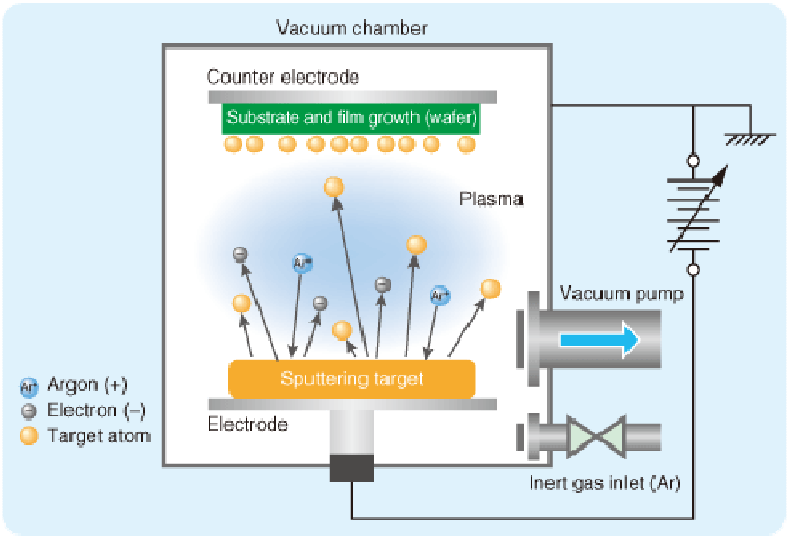

Figure II.5: *Schematic diagram of the sputtering method.*

II.3.2 Chemical and Electrochemical Techniques

II.3.2.1 Chemical Vapor Deposition (CVD)

Chemical vapor deposition (CVD) is a materials synthesis process whereby constituents of the vapor phase react chemically near or on a substrate surface to form a solid product. The main feature of CVD is its versatility for synthesizing both simple and complex compounds with relative ease at generally low temperatures. Liquid and solid reactants must be vaporized without decomposition at suitable temperatures and transported with a carrier gas through heated tubes to the reaction chamber, which complicates processing, especially in the case of reduced pressure systems. Materials deposited at low temperatures (*e.g.* below 600°C for silicon) are generally amorphous. Higher temperatures lead to polycrystalline phases. CVD has become an important process technology in several industrial fields [12]. Figure II.6 shows the deferent steps of CVD technique.

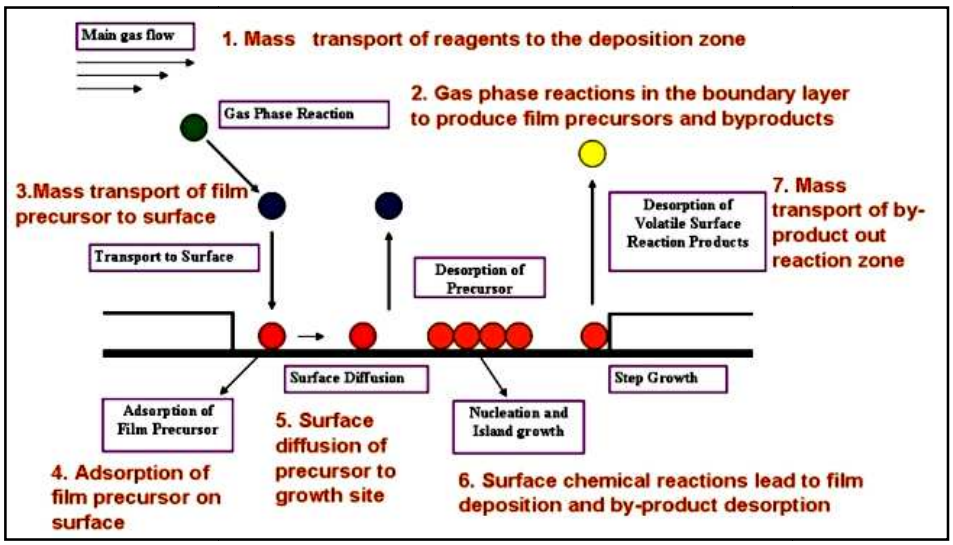

Figure II.6: *Deferent steps of chemical vapor deposition (CVD) technique.*

II.3.2.2 Chemical Bath Deposition (CBD)

Chemical bath deposition (CBD), also known as chemical solution deposition, has been known for more than a hundred years. This process can be easily implemented by immersing a substrate into a beaker, filled with an aqueous solution of chemical precursors, sitting on top of a hot plate (Figure II.7). The constituent ions are dissolved in a water solution, and the thin

films are produced through a heterogeneous surface reaction. In this technique, thin films can be deposited on different substrates like glass, ceramic, metallic…etc [13, 14].

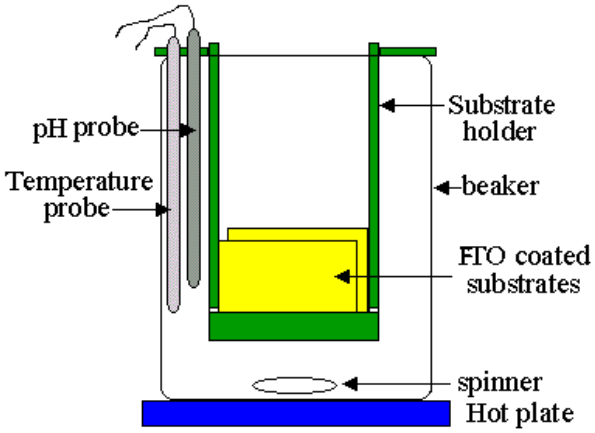

Figure II.7: *Schematics of chemical bath deposition (CBD) method.*

II.3.2.3 Sol-Gel Deposition

In Sol-Gel method the chemical precursors synthesized as a stable suspension (Sol). These "Sol" was transformed to a "Gel" during the gelling step result of chemical interactions between species in suspension and solvent, to give an expanded three-dimensional solid network through the liquid medium. The obtained gel is "wet" subsequently, it was transformed into dry amorphous material by removal of solvents (to obtain an air-gel) or by evaporation under atmospheric pressure (to obtain xerogel) [15]. Gel deposition at substrate can be performed from two different processes:

✓ Spinning (spin-coating, Figure II.8 a): in this process gel pouring on a rotated substrate by a spin coater. Excess gel is ejected under the effect of centrifugal force, and the deposition thickness depends of substrate rotational velocity, and deposition time [16].

✓ Dipping (dip-coating, Figure II.8 b): this process is less used than spin-coating. The substrate is dipped in the solution then it is withdrawn, this allows adhering gel at the substrate surface. The substrate is dried after each dipping process. Steps listed above must be repeat numerous times to obtain the desired film thickness [17]. Finally, the deposit material is dried and annealed for crystallization.

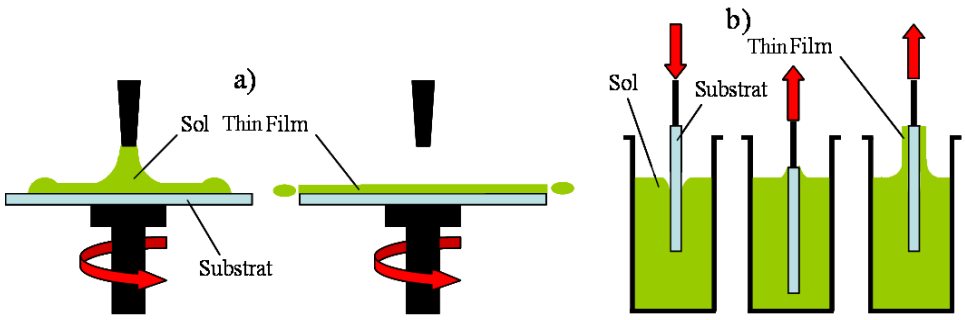

Figure II.8: *Schematics of sol-gel technique: (a) spin coating process; (b) dip coating process.*

II.3.2.4 Spray Pyrolysis

In this technique, the reaction between the clusters of the desired vapor atoms and substrate is thermally stimulated by elevated temperature. The sprayed droplets on reaching the hot substrate undergo pyrolytic decomposition and form a single crystal or cluster of crystallites of the product. The other volatile by products and excess solvents escape in the vapor phase. The thermal energy for decomposition, subsequent recombination of the species, sintering and recrystallisation of the crystallites is proved by hot substrate. The films are general strong and adherent, mechanically hard, pinhole free and stable with temperature and time, and the morphology of films is general rough [12]. Figure II.9 presented a schematics of spray pyrolysis showing its various parts.

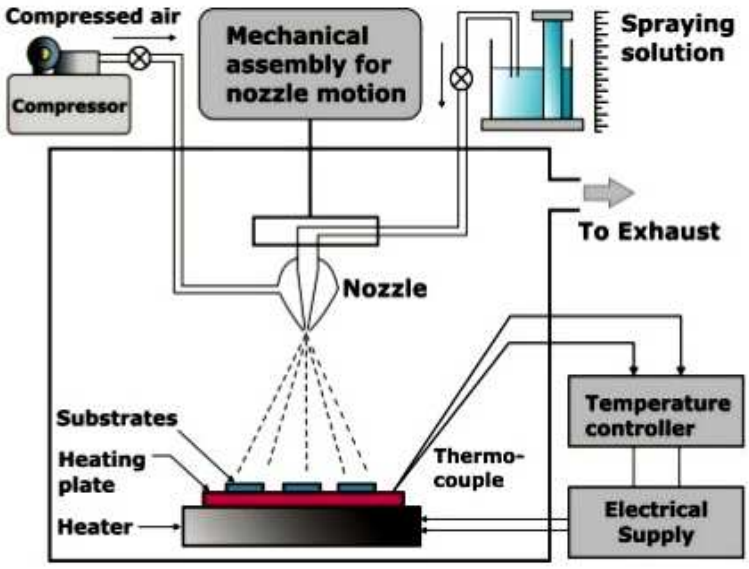

Figure II.9: *Schematics of spray pyrolysis showing its various parts.*

II.4 Ultrasonic Spray Method

Ultrasonic atomization technology's unique advantage is based on two features: its ability to generate very small droplets of an extremely narrow range diameter size, and its ability to apply these droplets gently on the substrate with minimum "bounce back" from the target surface. These features enable superior transfer coefficients when compared with conventional coating technologies, providing high-quality functional coatings at significantly lower cost. Figure II.10 shows ultrasonic spray experimental set-up schematic. In Figure II.10, the main parts in the ultrasonic spray deposition system are:

1. **Ultrasonic Generator:** it generates ultrasonic waves at frequency of about 40 KHz, this frequency value permits to transfer the solution into fine droplets at 40 µm of diameter.
2. **Solution Flow-meter:** it is used to control solution amount that passes to the atomizer.
3. **Reaction Chamber:** it is used to save the main set-up parts and to ejecting reactions gazes through an exhaust.
4. **Atomizer (nozzle):** it mainly role is the transformation of solution to fine droplets using ultrasound waves. It is placed on a holder and directed to the substrate. The distance nozzle-substrate can be adapted using a distance controller.
5. **Substrate Holder:** it is a ceramic plate, where the substrate is placed, surrounded by a cylinder to keep the solution droplets; it is heated using Joule effect to heating the substrate, the plate temperature is controlled by aiding a thermocouple.
6. **Temperature Controller:** it is used to control the plate temperature.

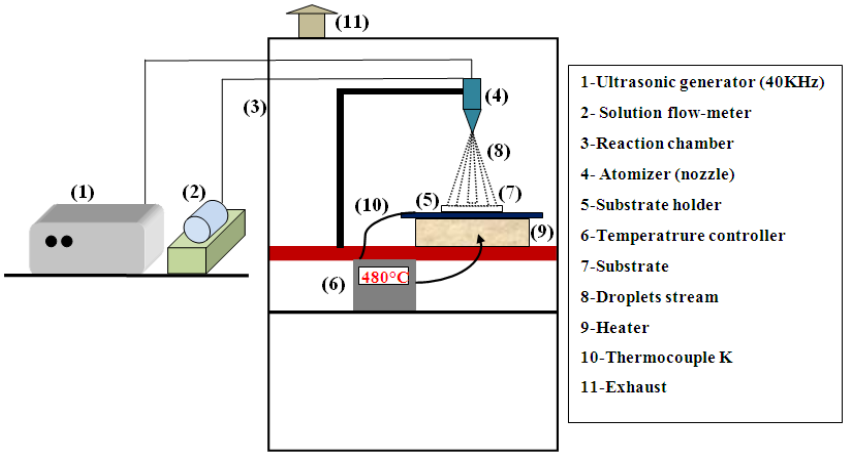

Figure II.10: *Ultrasonic spray experimental set-up schematic.*

II.4.1 General Principle of the Spray Process

A solution of different reactive compounds is sprayed using an atomizer, on a heated substrate. The substrate temperature allows activation of the chemical reaction between the compounds [18]. The experiment can be carried out in air, [19] and may be prepared in a vessel (or in a reaction chamber) under vacuum, approximately 50 Torr [20]. The films formation by ultrasonic spray method can be summarized as follows:

- Formation of the droplets at the atomizer outlet.
- Decomposition of the of precursors solution on the substrate surface and then activation of chemical reaction between the compounds.

In an ultrasonic spray method, drop size is governed by the frequency at which the nozzle vibrates, the surface tension and density of the liquid being atomized. Frequency is the predominant factor. Ultrasonic Coatings has a better control of process variables such as flow rate and droplet size means greater coating efficiency [21].

II.5 Characterization Methods

II.5.1 X-Ray Diffraction

X-ray diffraction (XRD) is one of the most important characterization tools for studying crystalline materials. XRD detects and analyses the diffracted X-rays from the crystallographic planes of the sample. This technique is mainly used for the chemical phase identification of both mono- and poly-crystalline unknown phases in a mixture. Moreover, XRD is used to determine structural properties like crystal structure, lattice parameters, interplaner spacing *d* and grain size. In this technique, the sample is bombarded with X-rays to produce a diffraction pattern which in turn are recorded and analyzed. Thus, the X-ray diffraction data obtained is compared with Joint Committee Power Diffraction Standards (JCPDS) data to identify the unknown material [22-24]. Figure II.11 shows the schematics of X-ray diffractometer. Interplaner spacing *d* can be calculated using Bragg's law:

$$n\lambda = 2d_{hkl}\sin\theta \qquad \text{(II.1)}$$

where, d_{hkl} is the interplaner spacing, Θ is diffraction angle (Bragg angle), λ is the X-ray wavelength and *n* is the diffraction order [22-24].

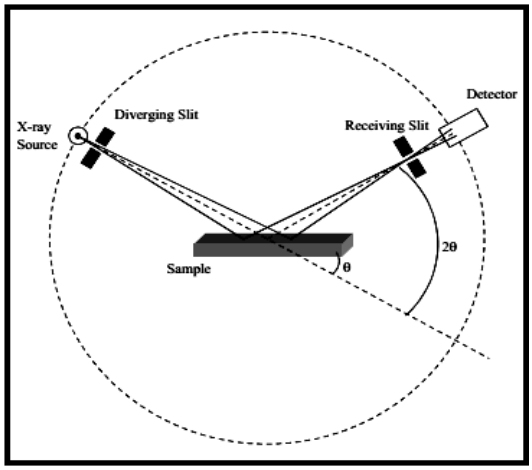

Figure II.11: *Schematics of X-ray diffractometer.*

III.5.2 Scanning Electron Microscope SEM

Scanning electron microscope (SEM) is an instrument used to observe the morphology of the solid sample [25]. When an electron strikes the atom, variety of interaction products are evolved. Scattering of electron from the atom electrons results into production of backscattered electrons and secondary electrons. Electron may get transmitted through the sample if it is thin. Primary electrons with sufficient energy may knock out the electron from the inner shells of atom and the excited atom may relax with the liberation of Auger electrons or X-ray photons. All these interactions carry information about the sample. Auger electron, ejected electrons and X-rays are energies specific to the element from which they are coming. These characteristic signals give information about the sample chemical identification and composition [26, 27]. The diagram of scanning electron microscope is shown in Figure.II.12.

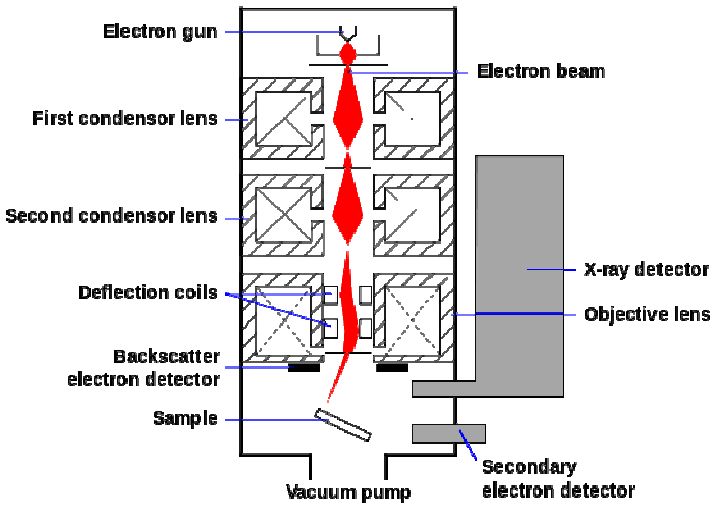

Figure.II.12: *Diagram of scanning electron microscope.*

II.5.3 Fourier Transform Infrared Spectroscopy (FTIR) Analysis

FTIR stands for Fourier Transform Infra-Red, the preferred method of infrared spectroscopy. In infrared spectroscopy, IR radiation is passed through a sample. Some of the infrared radiation is absorbed by the sample and some of it is passed through (transmitted). The resulting spectrum represents the molecular absorption and transmission, creating a molecular fingerprint of the sample. FTIR is used to identify unknown materials, determine the quality or consistency of a sample and also determine the amount of components in a mixture [28]. In FTIR method, the measured signal is decoded via the well-known mathematical technique called Fourier transformation. This transformation is performed by the computer which, then, presents the user with the desired spectral information for analysis. Figure II.13 shows the schematics of FTIR spectrometer [28].

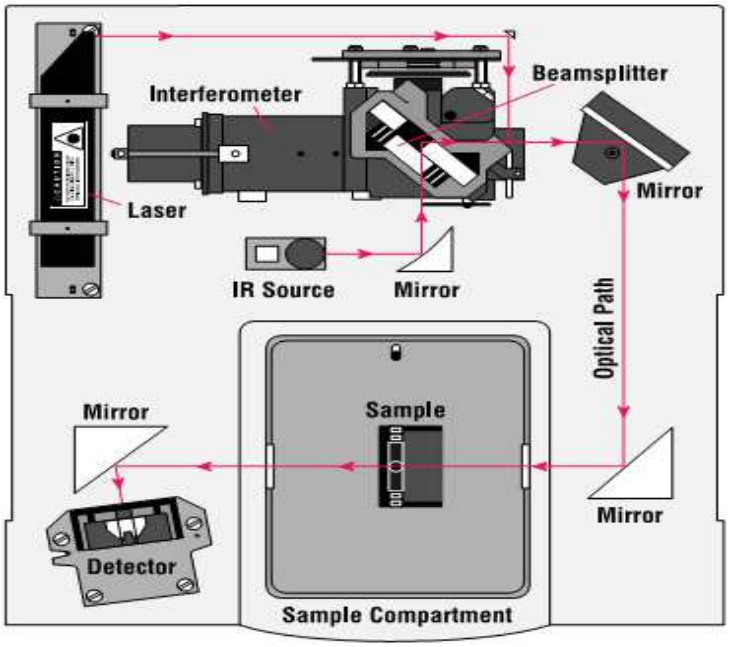

Figure II.13: *A Simple FTIR Spectrometer Layout.*

II.5.4 Photoluminescence

Photoluminescence spectroscopy (PL) is a contactless, nondestructive method. It is used primarily to investigate the electronic structure of materials. PL is the spontaneous emission of light from a material under optical excitation. In essence, laser light is directed onto a sample, where it is absorbed occurring the material photo-excitation (electron jumps to

a higher electronic state: from valence band to conductive band), then, the excited electron will release energy (photon) as it relaxes and returns to back to a lower energy level. The emission of light through this process is photoluminescence (see Figure II.14 (a)). The laser used in PL must be monochromatic and have photon energy greater than gap energy of the sample. PL investigations can be used to characterize a variety of material parameters such as band gap determination, crystal defects (such as atomic vacancies and substitutions), impurity levels, recombination mechanisms and material quality. A typical PL set-up is shown in Figure II.14 (b) [29-31].

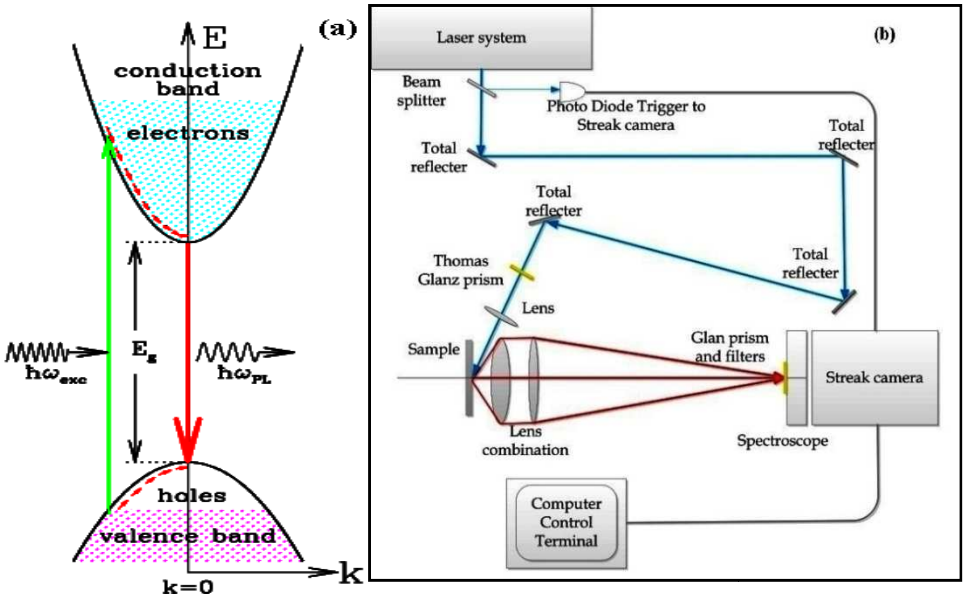

Figure II.14: *(a) Schematic band diagrams for the photoluminescence processes and (b) the experimental set-up for PL measurement.*

II.5.5 Hall Effect

Hall effect is an important diagnostic tool for the characterization of semiconductors materials. It provides a direct determination of both the sign of the charge carriers (electron or holes) and their density in a given sample. The basic setup is shown in Figure II.15. Hall effect occurs because a charged particle moving in a magnetic field is subject to the Lorentz force given by:

$$\vec{F} = e\vec{v} \times \vec{B} \qquad F = evB\sin\theta \tag{II.2}$$

where B is the magnetic field, θ is the angle between B-field and velocity vector v, e is the elementary charge and v is the particle velocity. The basic Hall measurement is performed on

a semiconductor bar with an electric field *E* applied along its long axis, and magnetic field *B* applied perpendicular to it [32, 33].

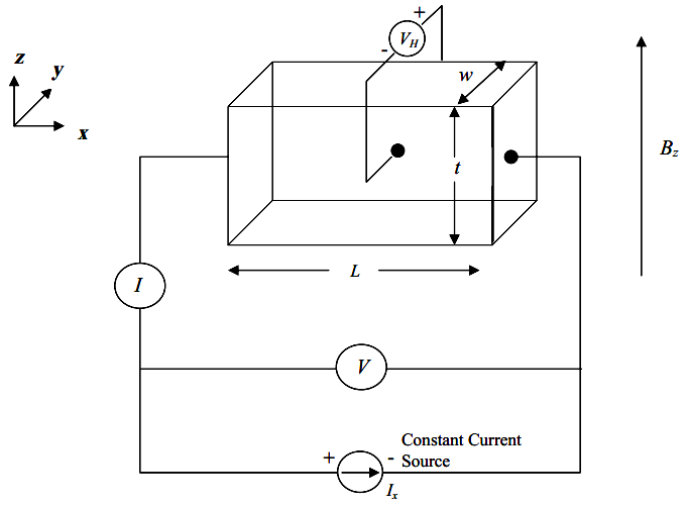

Figure II.15: *Hall voltage circuit.*

A useful measurement concept is Hall voltage (V_H), which is defined as:

$$V_H = \frac{-I_x}{|e|}\frac{B_z}{Nt} \quad (\text{n}-\text{type}) \quad \text{or} \quad V_H = \frac{+I_x}{|e|}\frac{B_z}{pt} \quad (\text{p}-\text{type}) \qquad \text{(III.3)}$$

where I_x is the current in the *x*-direction, B_z is the magnetic field in the *z*-direction, *N* or *p* is the carrier concentration per cm^3 and *t* the sample thickness. Since V_H, B_z, I_x and *t* are all known (by measurement), it is possible to solve for the carrier concentration *N* or *p*, and determine whether the sample is *n*-type or *p*-type [32-33].

II.5.6 Four Probes Method

The most common way of measuring the resistivity of a semiconductor material is by using a four-point collinear probe. This technique involves bringing four equally spaced probes in contact with a material of unknown resistance. The probe array is placed in the center of the material, as shown in Figure II.16. The two outer probes (1 and 4) are used for sourcing current *I* and the two inner probes (2 and 3) are used for measuring the resulting voltage drop *V* across the surface of the sample. Typical probes spacing "a" is ~1 mm [34, 35].

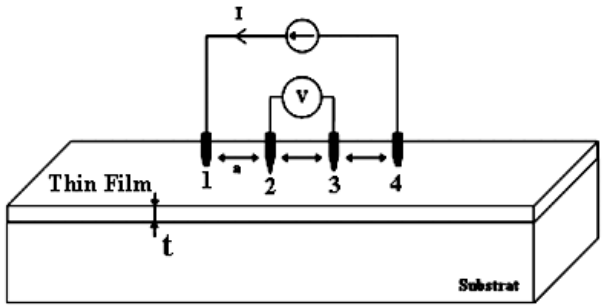

***Figure II.16**: Four-Point Collinear Probe Resistivity Configuration.*

Resistivity value is related to the measurement ratio (***V/I***). The voltage drop *V* is given as a function of the current injected value *I* by the relation:

$$V = \left(\frac{\ln 2}{2\pi}\right)\frac{I}{t}\rho \tag{II.4}$$

where, ρ is the film resistivity and *t* is the film thickness. The quantity (***ρ/t***) has unit of resistance named the sheet resistance $\boldsymbol{R_{sh}}$, its unit is Ω/□ (ohms per square) [34, 35].

$$R_{sh} = \frac{\rho}{t} \tag{II.5}$$

Resistivity can be calculated as follow:

$$\rho = \frac{2\pi}{\ln 2}\left(\frac{V}{I}\right)t = 4.53\left(\frac{V}{I}\right)t \tag{II.6}$$

Where 4.53 is a correction factor. Sheet resistance value can be derived from the last relation as follow:

$$R_{sh} = 4.53\frac{V}{I} \tag{II.7}$$

II.5.7 Optical Characterization by Ultraviolet and Visible (UV-VIS) Spectroscopy

UV-VIS spectroscopy exploited electromagnetic radiations from190 nm to 800 nm (ultraviolet region UV: 190-400 nm and visible region VIS: 400-800 nm) to give a spectrum

represents the transmission, reflection or absorption of the film. transmittance spectrum can be obtained by using a double beam UV-VIS spectrophotometer as shown in Figure II.17.

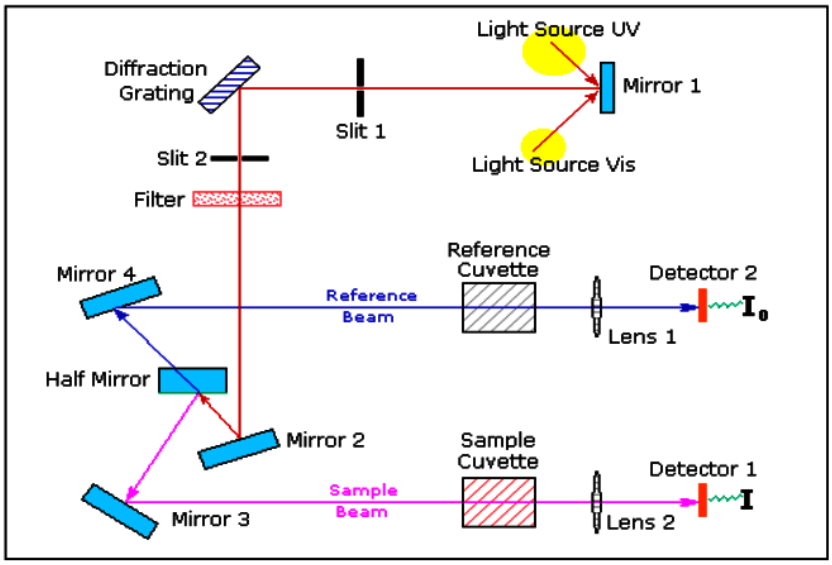

Figure II.17: *Schematic of UV-VIS spectrophotometer.*

UV-VIS spectrometry provides information about the film optical properties. By exploiting transmittance curve, it is possible to calculate the film thickness, the optical band gap and the refractive index. Figure II.18 shows the general form of transmittance spectrum obtained for SnO_2 thin film deposited on glass substrate [36]:

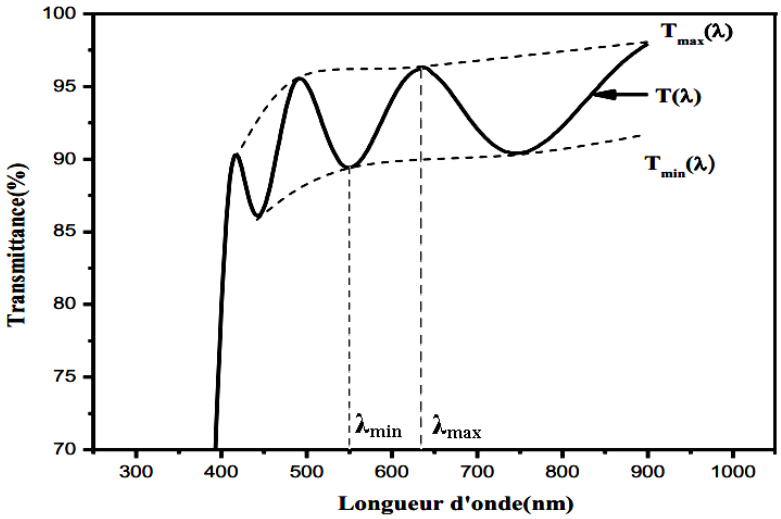

Figure II.18: *Transmittance spectrum of SnO_2 thin film.*

The absorption coefficient (α) can be determined using Beer-Lambert law:

$$T = \exp(-\alpha t) \tag{II.8}$$

where; α is the absorption coefficient and t is the film thickness. Eq. II.8 can be written as:

$$\alpha(cm^{-1}) = \frac{1}{t} ln\left(\frac{100}{T(\%)}\right) \tag{II.9}$$

This approximation relation is established by neglecting the reflection at all interfaces: air/film air/substrate and film/substrate [37]. α value near the absorption edge (at the interval $\alpha > 10^4 cm^{-1}$ *i.e.* UV) provides key information about the film's optical band gap. The energy gap E_g can be found from the well known relation Tauc's relation (see Figure II.19) as follow:

$$(\alpha h\upsilon)^2 = B\left(h\upsilon - E_g\right) \tag{II.10}$$

where; B is a constant, $(h\upsilon)$ is the photon energy and E_g is the band gap energy of the film.

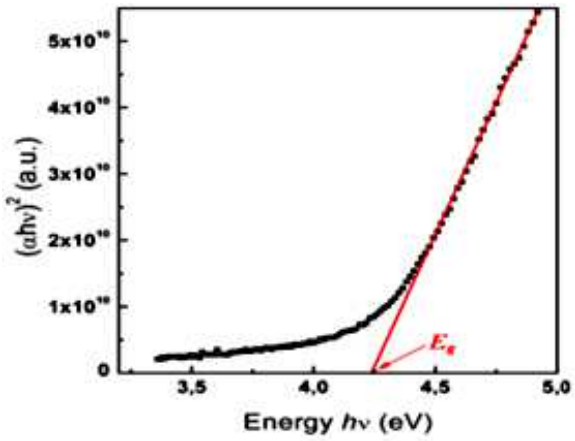

Figure II.19: *Plot of $(\alpha h\upsilon)^2$ vs. $(h\upsilon)$.*

II.5.8 Thickness Determination: Interference Method (Swanepoel Method)

Swanepoel proposed a method based on the idea of Manifacier et al. [38]. Swanepoel's analysis uses the interference fringes extremes of transmission spectrum to derive the refractive index and the thickness. If film thickness ***t*** is not uniform or is slightly tapered, all interference effects are destroyed and the transmission is a smooth curve as shown by the dotted curve ***T*** in Figure II.18. If the thickness t is uniform, interference effects give rise to the

spectrum shown by the full curve in Figure II.18. Fringes in the curve can be used to calculate film refractive index ***n*** and film thickness ***t***. Film refractive index in the transparent, weak and medium absorption regions can be expressed as [39, 40]:

$$n = \sqrt{N + \sqrt{N^2 + n_s^{\,2}}} \tag{II.11}$$

where n_s is the substrate refractive index. In transparent region (α=0) N can be given by the next equation:

$$N = \frac{2n_s}{T_m} + \frac{n_s^2 + 1}{2} \tag{II.12}$$

Whereas, in the spectral region of weak and medium absorption ($\alpha \neq 0$), N can be given by the following relation:

$$N = 2n_s\left(\frac{T_M - T_m}{T_M T_m}\right) + \frac{n_s^2 + 1}{2} \tag{II.13}$$

Where, T_M and T_m are the transmission maximum and the corresponding minimum at a certain wavelength λ. If n_1 and n_2 are the refractive indices at two adjacent maxima (or minima) at $\lambda_1$and λ_2, the film thickness can be calculated by the following expression [40, 41]:

$$t = \frac{\lambda_1 \lambda_2}{2(\lambda_1 n_2 - \lambda_2 n_1)} \tag{II.14}$$

Conclusion

As discussed in the previous chapter, thin films can be deposited by using several techniques such as Evaporation, pulsed laser deposition, Sputtering, chemical vapor deposition , sol-gel and spray pyrolysis. Among these techniques, ultrasonic spray method may be the most convenient technique because of its simplicity, low cost, easy to add doping materials and promising for high rate and mass production capability of uniform large area coatings in industrial applications. Also, Characterization is an important step in the development of new materials. The complete characterization of TCOs material consists of structural and surface characterization, optical characterization and electrical characterization which have strong bearing on the properties of materials.

In this chapter, the experimental steps, used to deposit our films, will be described. Then, the experimental results, obtained by the analysis of the elaborated SnO_2: F thin films, will be introduced. In this work, a focus is on the structural, optical and opto-electrical properties of undoped and fluorine doped SnO_2 thin films prepared by ultrasonic spray method. The effect of fluorine doping and film thickness on the previous properties of FTO films will be investigated in order to determine the suitable properties that make our films applicable as possible. The obtained results will be compared with the specified results presented by several researchers.

III.1 Deposition of Undoped and Fluorine Doped SnO_2 Thin Films by Ultrasonic Spray

III.1.1 Ultrasonic Spray Deposition System

Figure III.1 shows the ultrasonic spray deposition system of VTRS (Laboratoire de Valorisation et Téchnologie des Resources Sahariennes) laboratory in University of Eloued. All the studied SnO_2 samples in this work were prepared using the mentioned system.

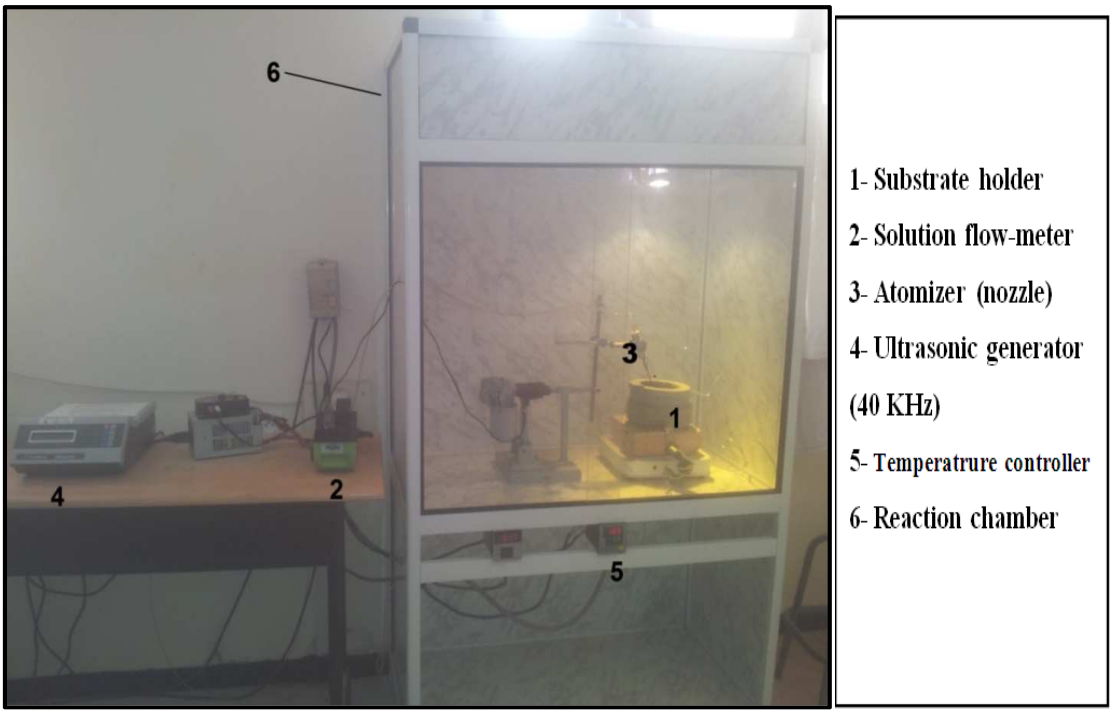

Figure III.1: *Photo of ultrasonic spray deposition system of VTRS laboratory.*

III.1.2 Substrate

Microscopic glass slides (Ref 217102) from CITOTEST were used as substrates. The glass slides, shown in Figure III.2, have dimensions of 75×25×1.1 mm^3 (for more information about the used glass see Appendix A).

Thin films quality depends on large number of parameters. One important parameter is the substrate surface state, hence, glass slides must be well cleaned and all contamination kinds such as grease and dust must be pulled out from their surfaces. The substrates were cleaned with alcohol and distilled water then blow-dried with nitrogen gas.

Figure III.2: *Microscopic glass slide used as substrates.*

III.1.3 Tin and Fluorine Sources

Stannous chloride ($SnCl_2$, $2H_2O$) was used as a precursor for tin. Also, it is known as Tin (II) chloride that forms a stable dihydrate. It is a white crystalline solid or powder as shown in Figure III.3 (a).

Ammonium fluoride was used as a precursor for fluorine. Ammonium fluoride is inorganic compound with the formula NH_4F. It adopts the wurtzite crystal structure, in which both the ammonium cations and the fluoride anions are stacked in layers, each being tetrahedrally surrounded by four of the other. It crystallizes as small colorless prisms as Figure III.3 (b) shows, having a sharp saline taste, and is exceedingly soluble in water.

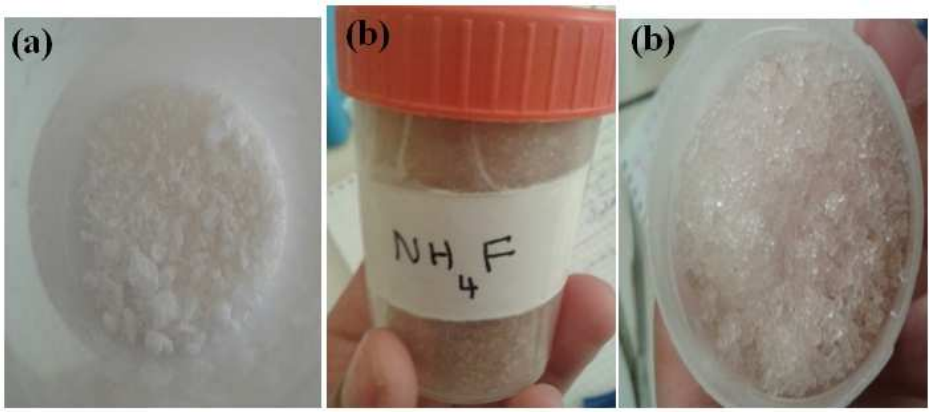

Figure III.3: *(a):Photo of the used stannous chloride ($SnCl_2$, $2H_2O$). (b):Photo of the used ammonium fluoride.*

III.1.4 Solutions Preparation

SnO_2 thin films were prepared from a solution of tin dichloride ($SnCl_2$, $2H_2O$). The precursor was dissolved in double distilled water and methanol in volume ratio 1:1. Mass of 1.1282 g tin dichloride was dissolved in 50ml of solvent to obtain a starting solution with molar concentration of about 0.1 M. In the basic solution, it is necessary to eliminate the problems of solubility and phase segregation, where the different components precipitate at different times. To overcome this and to obtain homogeneous solutions, we recommend to add, during preparation, a small amount of acid and in our work a few drops of hydrochloric acid (HCl) is used. The mixture solution was stirred at room temperature for half an hour to yield a clear and transparency solution.

Fluorine doping was achieved by adding, appropriate amount of ammonium fluoride (NH_4F) dissolved in doubly distilled water, to the starting solution. The obtained blend was used as a stock solution for spray ultrasonic. The added fluorine amounts were evaluated by weight percent (*wt.* %) unite. The F concentration in the solution was varied from 0 to 12 *wt.*% of course by adding appropriate amount of (NH_4F). Table III.1 summarizes the parameters used in films preparation. The basic chemical laws used to calculate the chemical magnitude with detailed calculation steps are illustrated in Appendix B.

Table III.1: *The parameters used in films preparation*.

Mass of tin dichloride	Solvent volume	Solution molarity	Fluorine concentration	Substrates temperature	Deposition time	Nozzle-substrate Distance
1.1282 g	50 ml	0.1 M	0-12 *wt.*%	480 °C	1-5 min	5 cm

Substrates temperature was fixed at 480 °C. The starting solution and blend solution were sprayed separately on heated glass substrates by spray ultrasonic system to obtain undoped SnO_2 and F doped SnO_2 thin films.

Chemical reactions, taking place in spray process, are as follow:

In the solution:

$$SnCl_2 + H_2O + CH_3 - OH \rightarrow SnO + 2HCl^{\uparrow} + CH_3 - OH$$

Reaction of undoped SnO_2 deposition (on the heated substrate):

$$SnO + CH_3 - OH + \frac{1}{2}O_2 \xrightarrow{480°C} SnO_2 + CH_3 - OH^{\uparrow}$$

whereas the reaction occurs between fluorine F and SnO_2 is:

$$SnO_2 + xF \rightarrow Sn^{+4}F_x^{-1}O_{2-x}^{-2}\left[xe^{-}_{BC}\right] + \frac{1}{2}xO_2^{\uparrow}$$

Note that the decomposition reaction, in the gas phase, occurring on the substrate surface is an endothermic reaction which require relatively high temperatures to achieve the decomposition of solutions used (droplets) arriving on heated substrates.

III.1.5 Thin Films Deposition Steps

After substrate cleaning and solution preparation the films deposition steps are taking place as follow:

1-The substrate is placed on the Substrate holder then the heater is being worked until arriving to the desired temperature 480 °C.

2-When spray process starts; the prepared solution is sprayed ultrasonically on heated substrate (at temperature 480 °C). Temperature allows the activation of the chemical reaction, and certain by products (volatile components) will be immediately disposed off.

3-The deposition time is varied from 1 min to 5 min to obtain different film thicknesses.

4- At the end of spraying step, the substrate is let on the holder to cool down progressively until ambient temperature.

5- Progressive heating or cooling is used to avoid thermal shocks that create glass breaking. It also ameliorates films homogeneity.

6- Finally, we obtain glass samples coated by SnO_2 and F doped SnO_2 thin films as Figure III.4 shows:

Figure III.4: *Glass coated by F doped SnO_2 thin film.*

7- To study the effect of fluorine doping: all used films were taken at the same deposition time (3 min deposition).

8- Note that all measurements were carried out at room temperature (*rt*).

III.2 Structural Analysis

Structural characterizations are carried out using X-ray diffraction (XRD) with an X-ray diffractometer (BRUKER-AXS type D8) under Cu Ka (λ=1.5405 Å) radiation.

III.2.1 Crystalline Structure

The X-ray diffraction pattern of F (0–12 *wt.*%) doped SnO_2 thin films prepared by ultrasonic spray are shown in Figure III.5. as it can be seen the diffraction peaks were observed at 2θ=26.68°, 33.97°, 37.8°, 51.79°, 61.72° and 65.95° which are related to the following plans: (110), (101), (200), (211), (310) and (301) respectively.

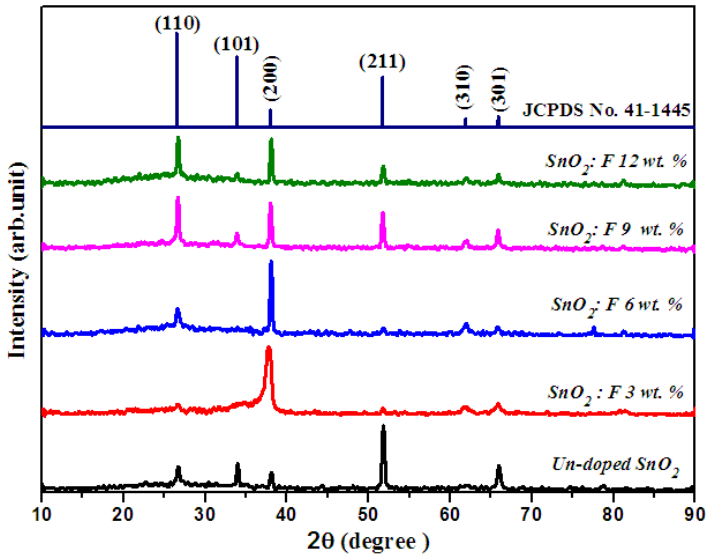

Figure III.5: *XDR patterns of F (0–12 wt.%) doped SnO_2 thin films.*

For all deposited films, major peaks corresponding to the tetragonal SnO_2 (JCPDS No. 41-1445) were observed. It can be seen that all the films are polycrystalline and having SnO_2 tetragonal rutile structure ($P4_2/mnm$ (136)), and no phase corresponded to fluorine was observed. The peaks of the undoped SnO_2 were indexed to the tetragonal SnO_2 structure [1, 2] with (211) as very prominent plane whereas four close lying reflections (110), (101), (200), and (301) were also evidently indicating the polycrystalline nature of the same film; the polycrystallinity may be due to the use of water with the solvent [3]. Moreover, single significant (200) diffraction peak, with height intensity, was observed for the 3% and 6 *wt.*% doped SnO_2 film which indicating preferential orientation along the (200) plane. For the heavily Fluorine doped SnO_2 thin films (9 and 12 *wt.*%) one cannot make a significant difference between them whereas all the diffraction peaks mentioned above reappear again.

III.2.2 Texture Coefficient *TC(hkl)*

The texture coefficient *TC(hkl)* represents the texture of the particular plane, deviation of which from unity implies the preferred growth. The different texture coefficient *TC(hkl)* have been calculated from the X-ray data using the well-known formula [4]:

$$TC(hkl) = \frac{I(hkl)/I_0(hkl)}{N^{-1}\sum_n^N I(hkl)/I_0(hkl)} \qquad \text{(III. 1)}$$

where *I(hkl)* is the measured relative intensity of a plane *(hkl)*, $I_0(hkl)$ is the standard intensity of the plane *(hkl)* taken from the JCPDS data, *N* is the reflection number and *n* is the number of diffraction peaks. *TC(hkl)* values of all the films for (110), (200) and (211) with increase in F concentration are recapitulated in Table III.2. The peaks were less than unity confirming the poly-crystalline nature of the films. However, the 3 and 6 *wt.*% F doped SnO_2 films presented a possible oriented growth along the (200) plane direction.

III.2.3 Lattice Constants

The lattice constants '*a*' and '*c*', for the tetragonal phase structure is determined from XRD results using the following equation [5]:

$$\frac{1}{d_{hkl}^2} = \frac{h^2 + k^2}{a^2} + \frac{l^2}{c^2} \qquad \text{(III. 2)}$$

where d_{hkl} is the inter-planar distance, *(hkl)* are the Miller indexes and '*a*' and '*c*' are the lattice constants. The calculated and standard lattice constants are illustrated in Table III.2.The lattice parameters of undoped SnO_2 thin film are, a=b=4.720 Å and c=3.242 Å whereas the standard ones are a=b=4.737 Å and c=3.185 Å according to JCPDS data. Changes in *a* and *c* values may be attributed to F^- (ionic radius=1.17 Å) substitution of O^{2-} (ionic radius=1.22 Å) [6], see section I.13 in chapter I.

III.2.4 Crystallite Sizes *D*

The average crystallite sizes, given in the Table III.2, were calculated from highly textured peaks by using Scherrer's formula [7]:

$$D = \frac{0.9\lambda}{\beta \cos \theta} \qquad \text{(III. 3)}$$

where *D* is the crystallite size, β is the full width at half-maximum (FWHM) of the most intense diffraction peak, λ is the X-ray wavelength (1.54056 Å) and θ is the Bragg angle. Scherrer's equation applied to the most intense (211) and (200) diffraction lines for the undoped and F-doped films respectively. The variations of crystallite size with F concentration are shown in Figure III.6. For undoped film the crystallite size was about 24.74 nm whereas it was found to decrease only for 3 *wt.*% F doped SnO_2 and increased with increasing in F concentration as Table III.2 shows.

Table III.2: *Crystallite size, lattice parameters, TC (hkl) and dislocation density of SnO_2 and SnO_2: F films.*

Material	**Crystallite size *D* (nm)**	**Lattice constants (Å)**				***TC*(*hkl*) of plane**			**$\delta\times10^{15}$ (lines/m^2)**
		a	**$\Delta a= a-a_0$**	***c***	**$\Delta c=c-c_0$**	**(110)**	**(200)**	**(211)**	
Undoped SnO_2 film	24.740	4.720	-0.016	3.242	0.057	0.737	0.573	1.885	1.63
SnO_2: F 3 *wt.* %	11.579	4.766	0.029	3.143	-0.041	0.488	2.707	0.338	7.46
SnO_2: F 6 *wt.* %	26.467	4.724	-0.012	3.257	0.072	0.956	2.469	0.339	1.41
SnO_2: F 9 *wt.* %	27.644	4.727	-0.009	3.248	0.063	1.397	1.250	1.004	1.31
SnO_2: F 12 *wt.* %	28.165	4.722	-0.014	3.253	0.068	1.568	1.508	0.680	1.26

III.2.5 Dislocation Density δ

The growth mechanism involving dislocation is a matter of importance. Dislocations are imperfect in a crystal associated with the mis-registry of the lattice in one part of the crystal with respect to the other parts. Dislocations are not likely to play a major role in the variation of electrical resistance because an increase in dislocation density values gives rise to disorders, crystal defects in lattice and a decreasing crystallinity. The dislocation density (δ) is defined as the length of dislocation lines per unit area as defined in literature [8-11], which can be estimated from the following relation using the simple approach of Williamson and Smallman [8]:

$$\delta = \frac{1}{D^2} \qquad \text{(III. 4)}$$

where *D* is the crystallite size, the dislocation values were found to be in the range 1.26-7.46×10^{15} lines/m^2 for undoped and F-doped films as reported in Table III.2.

Figure III.6 shows the variation of the dislocation density δ as a function of F concentration. For undoped film δ was about 1.63×10^{15} lines/m^2. It is clear that δ increases only for 3 *wt.*% F doped SnO_2 and decreased with increasing in F concentration, this behavior can be explained by the change of the particle's size D with F concentration. Indeed, the smaller crystallites allow deposition in relatively large numbers and possibly the appearance of linear defect (dislocation) and their development throughout the growing structure.

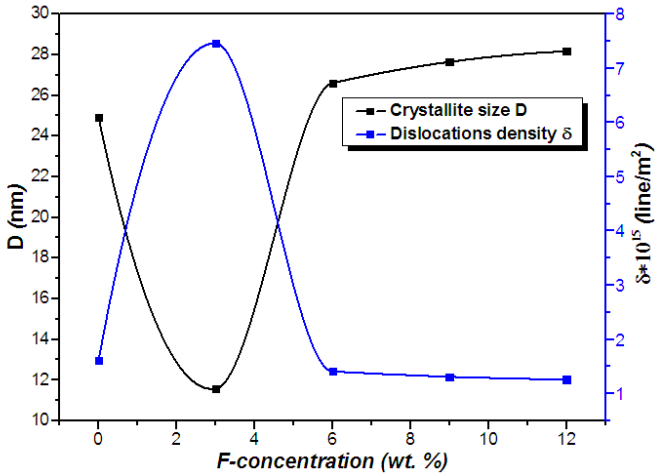

Figure III. 6: *Variations of crystallite size and dislocation density of FTO thin films as a function of F concentration.*

III.2.6 Thickness Effect on Structural Properties

The X-ray diffraction patterns of the SnO_2 films deposited by ultrasonic spry at different deposition time (*i.e.* different film thicknesses) as shown in Figure III.7.

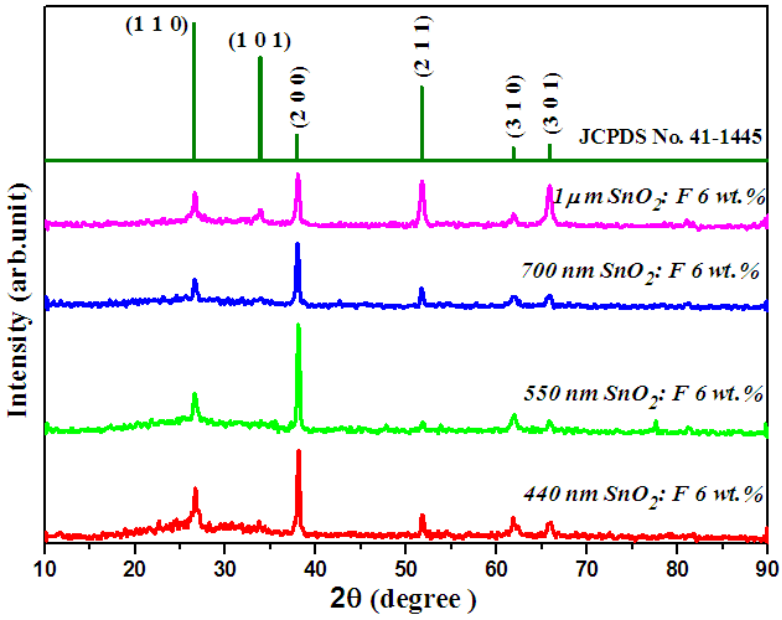

Figure III.7: *XRD patterns of F-doped SnO_2 films as function of film thickness.*

The XRD results of our SnO_2: F 6 *wt.* % thin films exhibited five peaks. For the F-doped films with thickness, less than (1 µm) the prominent (200) planes were observed. Other peaks

observed, with weak intensities, are (110), (211), (301) and (310). Further, it was observed that (110), (200), (211) and (301) planes are prominent for the film with 1µm thickness. In order to evaluate the preferred orientation of the SnO_2 films, we use the texture coefficient. *TC(hkl)* calculated values of the films for (110), (200) and (211) peaks are listed in Table III.3. The latter were less than unity confirming the polycrystalline nature of the films. It was observed that the film with thickness of about 1 µm has good growth along (101), (211) and (301) planes; this effect may be attributed to the increase in amount of tin sprayed on glass substrate due to increase in deposition time [12].

- **Thickness Effect on Lattice Constants**

The lattice constants '*a*' and '*c*', for the tetragonal phase structure are determined and illustrated in Table III.3. The calculated '*a*' values are slightly less than that given by JCPDS card; whereas, all values of the lattice constants '*c*' are marginally larger than that of JCPDS card.

- **Thickness Effect on Crystallite Sizes**

The crystallite sizes of SnO_2: F thin films for different thickness, given in the Table III.3. *D* sizes distributions are between 21.49-26.88 nm; as can be seen in Figure III.8 grain size plot for F doped films reveals a decrease with thickness increasing which may be attributed to film thickness effects [12].

Table III.3: *Crystallite size, lattice parameters, texture coefficients and dislocation density of SnO_2: F 6 wt. % for different film thickness.*

Material	**Thickness *t* (nm)**	**Crystallite size *D* (nm)**	**Lattice constants (A°)**				***TC*(*hkl*) of plane**			**$\delta\times10^{15}$ (lines/m^2)**
			a	**$\Delta a= a-a_0$**	***c***	**$\Delta c=c-c_0$**	**(110)**	**(200)**	**(211)**	
SnO_2: F (6 *wt.*%)	440	26.883	4.724	-0.013	3.236	0.051	0.295	2.384	0.266	1.38
	550	26.467	4.724	-0.013	3.260	0.075	0.233	3.262	0.145	1.43
	700	24.949	4.735	-0.002	3.228	0.043	0.245	2.550	0.313	1.61
	1000	21.492	4.733	-0.004	3.234	0.049	0.252	1.957	0.758	2.16

- **Thickness Effect on Dislocation Density**

Dislocation density for F-doped films at different thickness was calculated. The values were found to be in the range 1.38-2.16×10^{15} lines/m^2 as reported in Table III.3. As can be

seen, dislocation density increases with thickness increasing. It was observed that the films with 440 nm and 550 nm thickness have the less dislocation density which makes those films the best not only in structural properties but in electrical properties as well. The obtained values of dislocation density are comparable with values reported in literature [13] where the authors work deals with SnO_2: F deposited on glass substrates by electro-deposition and are less than those obtained by M. Ajili et al. [14] for SnO_2: F films deposited on glass substrates by spray technique. The variations of dislocation density δ as a function of film thickness are shown in Figure III.8.

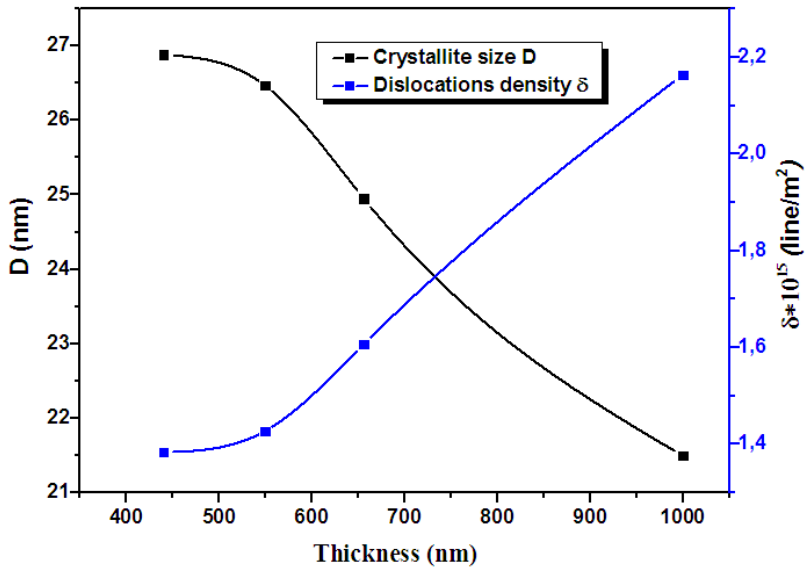

Figure III.8: *Crystallite size and dislocation density variations as function of film thickness for FTO films.*

III.3 Morphological Characterization

Morphology of the films deposited for various fluorine doping concentration (3, 6 and 12 *wt.* %) was analyzed by SEM (Jeol model JSM 6390 lv). SEM images of the films surface are given in Figure III.9 which shows uniform morphology with uniform grain sizes. Also it was seen, that the substrate is well covered with fine grains and homogeneous distribution. It is worth noting that sample doped at 12 *wt.* % present more agglomerations on surface than the others.

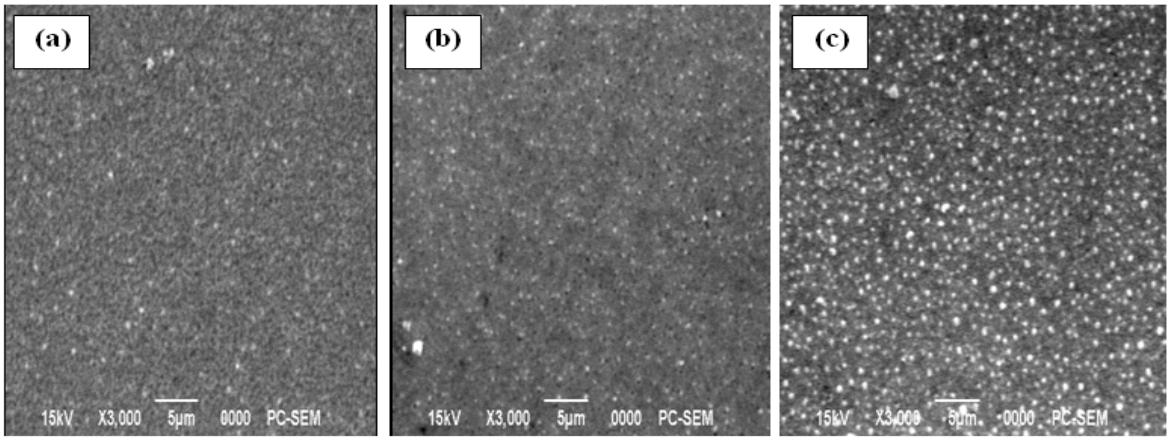

Figure III.9: *SEM images of SnO_2: F (3-12 wt. %): (a) 3 wt. %, (b) 6 wt. % and (c) 12 wt. %.*

III.4 Optical Analysis

Optical transmission spectra were obtained using an UV-visible spectrophotometer (Shimadzu, Model 1800) in spectral region 200–900nm.

III.4.1 Optical Transmission

The optical transmission $T(\lambda)$ measurements as a function of the wavelength of SnO_2 films prepared by ultrasonic spray are depicted in Figure III. 10 where we have gathered the undoped and doped F (0–12 *wt.*%) SnO_2 spectra.

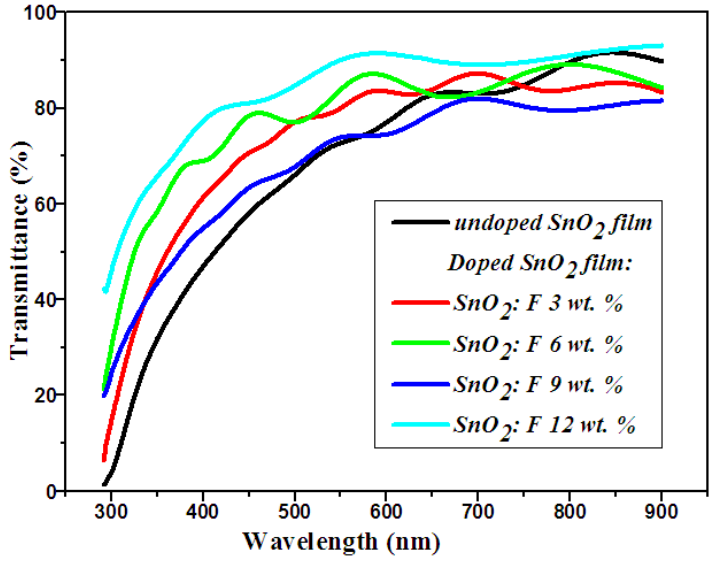

Figure III.10: *Optical transmittance plot of F (0–12 wt.%) doped SnO_2 thin films.*

As it can be seen, a height transparent spectra *T(λ)* of undoped SnO_2 in visible region, the average transmission is more than 74 % and the film exhibit significant oscillations in long wavelength; this oscillation may be due to the smooth of the top surface of undoped SnO_2 film which can generate interference phenomenon; even at nuked eye, one can see that the undoped SnO_2 lattice is very smooth. Then the transmission decreased because of the onset fundamental absorption in the region round 340nm. For the doped SnO_2 films, the value of transmission *T(λ)*, in the visible region, is located in the average 73.5–87.5 % revealing good agreement with transmittance value of fluorine doped tin oxide films mentioned in the literature [12, 15]. Transmission values exhibit slight increase upon the increasing the F doping amount as it shown in Figure III.10. The region of the absorption edge in the all layers due to the transition between the valence band and the conduction band is located between 300–340nm until 6 *wt.*%; in this region, the transmission decreased because of the onset fundamental absorption. One can note that the doping effect is clearly observed in the layer quality such as in the average between 300–340 nm; blue shift of the absorption edge was observed as function of doping level until 6 *wt.*% reveling Burstein–Moss effect [16, 17], then sleight return to the initial values of the absorption edge revealing the Roth effect [18] which indicates that the increasing of doping amount can change the lattice structure.

III.4.2 Thickness Determination

From the oscillation of the spectra, the thickness of the films (*t*) was determined by using the following equation [19]:

$$t = \frac{\lambda_1 \lambda_2}{2(n_1 \lambda_2 - n_2 \lambda_1)} \qquad \text{(III. 5)}$$

where $\boldsymbol{n}_1$ and $\boldsymbol{n}_2$ are the refractive indexes at the two adjacent maxima (or minima) at $\boldsymbol{\lambda}_1$ and $\boldsymbol{\lambda}_2$. The thickness of films was over than 550 nm in average as shown in Table III.4. It was observed that the thickness of the film does not present any trend with F concentration.

Table III.4: *Films thickness, transmittance and optical gap values for SnO_2 and SnO_2: F thin films.*

Material	Thickness *t* (nm)	T_{moy} (%)	*Eg* (eV)	Δ*Eg* (eV)
Undoped SnO_2 film	806	74.160	3.622	0
SnO_2: F 3 *wt.* %	935	79.951	3.846	0.224
SnO_2: F 6 *wt.* %	550	82.289	3.860	0.238
SnO_2: F 9 *wt.* %	877	73.540	3.785	0.163
SnO_2: F 12 *wt.* %	975	87.572	3.656	0.034

III.4.3 Optical Band Gap

The band gap (*Eg*) of pure SnO_2 is widely reported to be of direct transition in nature (3.87–4.3 eV) [20, 21]. The direct band gap of F doped SnO_2 films was determined from Tauc relation ($(\alpha h\upsilon)^2 vs. h\upsilon$) plot by extrapolating the linear region to α=0 [22] as seen in Figure III.11. It was found that the band gap increased with increase in level doping of F in SnO_2. The increase in band-gap may be attributed to the partial filling of the conduction band of tin oxide, resulting in a blocking of lowest states. This widening of the optical band gap is termed as Burstein–Moss shift [16, 17]. With further increase in the F concentration in the SnO_2 film (from 6 *wt.*% F onward) the band-gap of films begins to decrease revealing Roth effect [18] as it was mentioned in Table III.4.

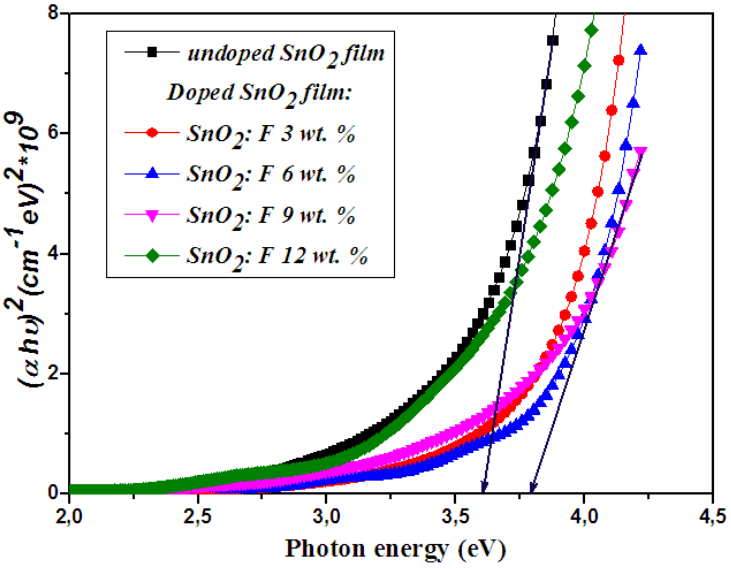

Figure III.11: *Band-gap estimation from Tauc relation of F (0–12 wt.%) doped SnO_2 films.*

III.4.4 Thickness Effect on Optical Properties

Figure III.12 shows UV–Vis transmittance spectra of SnO_2: F 6 *wt.*% thin films with various film thicknesses. The transmittance of all samples was more than 74% in the whole visible-light region (400-800 nm). Transmittance values, of SnO_2: F 6 *wt.*% thin films decrease with increasing film thickness; this effect is well expected from the Beer–Lambert law [23].

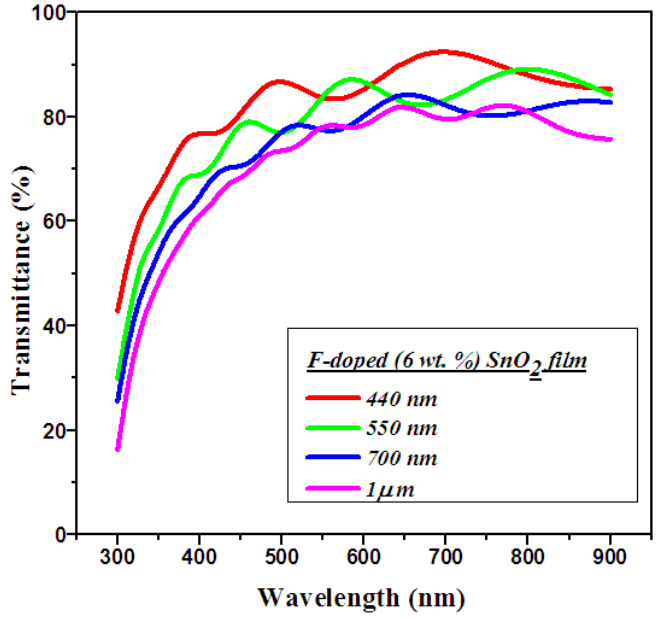

Figure III.12: *Transmittance spectra of SnO_2: F at 6 wt. % thin films for different film thicknesses.*

Table III.5 gathered transmittance values of fluorine doped SnO_2 thin films with film thickness (*t*). The thickness of the films was found to be between 440 nm and 1000 nm (1 µm) as listed in Table III.5. It is clear that the film thickness increases with increasing deposition time [6].

Table III.5: *Deposition times, film thicknesses, transmittance and E_g values for SnO_2: F 6 wt. % thin films.*

Material	**Deposition time (min)**	**Thickness *t* (nm)**	**Transmittance *T* (%)**	***E_g (eV)***
SnO_2: F (6 *wt.* %)	2	440	84.611	3.80
	3	550	82.289	3.86
	4	700	73.552	3.88
	5	1000	70.319	3.93

III.4.5 Thickness Effect on Band Gap Value

Figure III.13 shows the estimated optical band gap (E_g) of SnO_2: F 6 *wt.* % thin films with different film thicknesses. As recapitulated in Table III.5 E_g values of SnO_2: F 6 *wt.* % increases from 3.80 eV to 3.93 eV with increasing film thickness. The results are in good agreement with other results carried out in literature [12] and elsewhere [24].

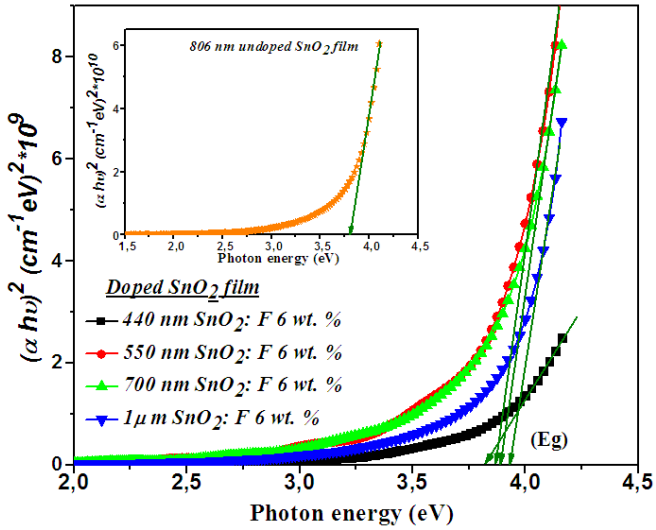

Figure III.13: *Band-gap estimation of SnO_2: F 6 wt. % thin films for different film thickness.*

III.4.6 Refraction Index

Refractive index *n* values of undoped and F-doped SnO_2 thin films are approximated to 1.99 on the visible wavelength average (400-800 nm), we noted that refractive index is not affected by fluorine doping augmentation. Our refractive index values are in good agreement with the values that found in the literature [25-27].

III.4.7 Growth Velocity

Growth velocity (*Gv*) of thin films can be estimated from the plot of films thickness upon time deposition as shown in Figure III.14. The later was found to be in the range of *Gv*=183 nm/min.

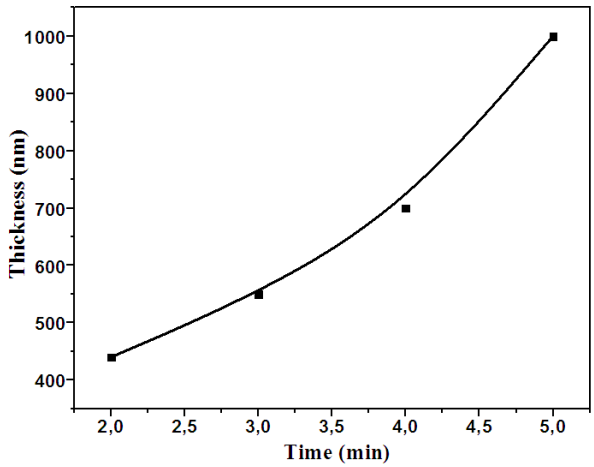

Figure III.14: *Plot of film thickness as function of deposition time for estimating growth velocity.*

III.5 Reflectance and plasma frequency

Optical reflectance spectra were obtained using an UV-visible spectrophotometer (UV, Lambda 35) in spectral region 200–2500 nm.

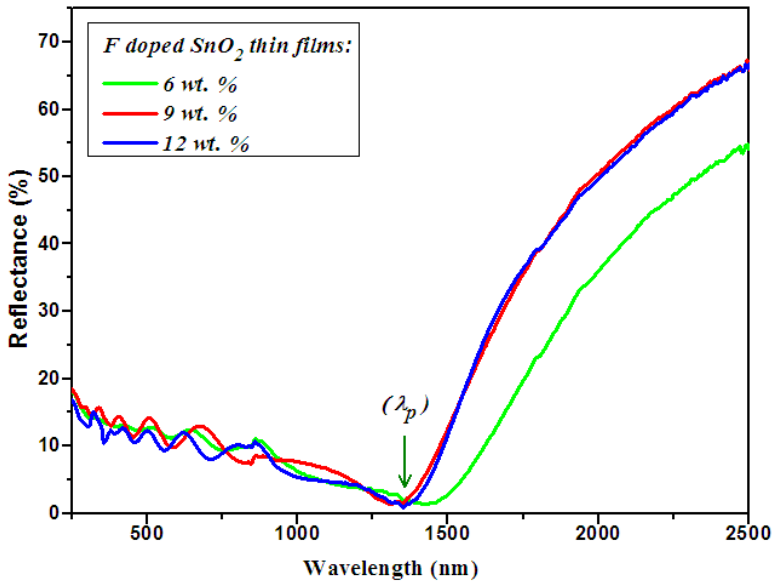

Figure III.15: *Spectral reflectance plot of F (6–12 wt. %) doped SnO_2 thin films.*

Reflectance spectra of SnO_2: F thin films deposited by ultrasonic spray, with various F concentrations, are shown in Figure III.15. As can be seen thin films have a weak reflectivity in UV-visible and near IR region especially at the plasma wavelength. Interferences

phenomena on the patterns are seen in UV-Vis region. The calculated IR reflectivity is found to be in the range of 55-67 %. Fluorine doping enhances films reflectivity in IR region.

Drude's model is generally used to analyze the decrease in the transmittance near the infrared region. Briefly, this model illustrates the drop in transmittance at the NIR region and it is associated with the plasma frequency (ω_p) expressed as [28, 29]:

$$\omega_p = \sqrt{\frac{Ne^2}{\varepsilon_0 \varepsilon_\infty m^*}} \qquad \text{(III.6)}$$

where N is the carriers concentration, e is the electronic charge, ε_0 is the permittivity of free space, ε_∞ is the high frequency permittivity and m^* is the effective mass. Plasma frequency is the frequency of periodic oscillations of charge density in conducting media [30]. For most TCO materials, the plasma frequency falls in the near-infrared part of the spectrum, that is why, the TCOs show good transparency to the visible light [31]. ω_p is proportional to the square root of the carrier concentration, an increase in carrier concentration leads to a decrease in transmission in the near-IR region. The plasma wavelength λ_p is expressed as [32]:

$$\lambda_p = \frac{2\pi c}{\omega_p} \qquad \text{(III.7)}$$

The plasma wavelength shifts towards the lower wavelength side due to increases in carrier concentration and then shifts towards the higher wavelength region due to a decrease in carrier concentration as seen in Figure III.15. Plasma frequency and plasma wavelength values are recapitulated in Table III.6.

Table III.6: *Plasma wavelengths, plasma frequencies and carrier concentration of SnO_2: F thin films.*

Material	**λ_p (*nm*)**	**ω_p (Hz)×10^{15}**	**Optical *N* (*cm^{-3}*)×10^{21}**
SnO_2: F 6 *wt.* %	1430	1.317	1.575
SnO_2: F 9 *wt.* %	1350	1.395	1.767
SnO_2: F 12 *wt.* %	1370	1.375	1.716

III.6 Characterization by FTIR Spectroscopy

FTIR transmission spectra were recorded using "Shimdzu IR Affinity 1" spectrometers (resolution 4 cm^{-1}, 10 scans). FTIR analysis has been performed on SnO_2 and SnO_2: F thin films. The results were plotted in transmission mode in the range of 390-1100 cm^{-1} and shown in Figure III.16

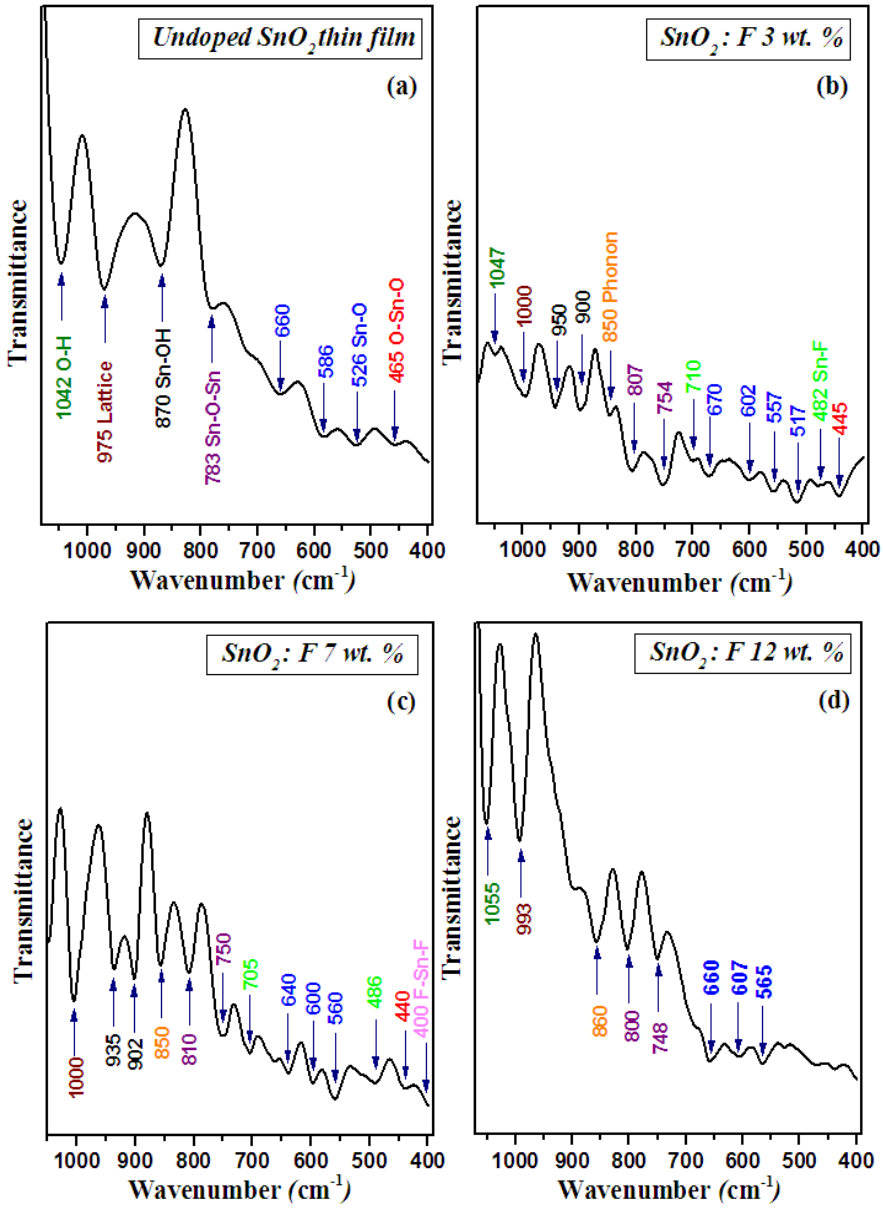

Figure III.16: *FTIR spectra of un-doped and F-doped SnO_2 films.*

FTIR study confirmed the formation of SnO_2 with characteristic vibration modes of Sn–O at 526, 586 and 660 cm^{-1} [33-35]and O–Sn–O at 465 cm^{-1} [34, 36-38]. All vibrations

modes at 500–700 cm^{-1} region are assigned to Sn–O stretching of tin oxide [33-35].The peak at 783 cm^{-1} can be assigned to Sn–O–Sn stretching vibrations [15, 39], while the peak at 850 cm^{-1} is due to the phonon vibration [38]. The peak at 870 $cm^{-1}$is due to Sn–OH bonds of the SnO_2 crystalline phase [15] and the peak at 975 cm^{-1} is due to lattice vibrations [39]. The strong IR bands at 1042 cm^{-1} can be assigned as the vibration mode of (O-H) group of residual water and alcohol [40].

After fluorine doping, two interesting phenomena have been observed which are a shift and appearance of others peaks related to fluorine incorporation. The first one (shift): the peaks at 975, 870 and 783 cm^{-1} shifted to, ~1000, ~900 and ~800 cm^{-1} respectively, because of fluorine doping. The second phenomenon is the appearing of Sn–F vibration mode at 482 cm^{-1} with weak peak intensity in SnO_2: F doped at 3 *wt.* % as Figure III.16 (b) shows; this peak intensity increases when F concentration reach 7 *wt.* % with another appearance of F-Sn-F vibration mode around 400 cm^{-1} as remarked in Figure III.16 (c), this result was carried out in literatures [15, 36, 41]. In addition, a weak peak at ~709 cm^{-1} appeared in SnO_2: F 3*wt.* % pattern and increases at 7*wt.* % fluorine doping level. This peak was attributed to Sn-F stretching mode vibration as will be demonstrated in the section IV.2 of Chapter IV. Those peaks related to Sn-F and F-Sn-F vibrations disappear when F doping level reach 12 *wt.* % as seen in Figure III.16 (d).

III.7 Sheet resistance and Hall Effect

Carrier concentration determined using Hall Effect measurement setup (Scientific Equipments, Model: EMU.50) and sheet resistance was measured with four-point probe on 1x1cm^2 sample sheet. All F doped SnO_2 thin films were conducting at room temperature with resistivity values much less than of undoped SnO_2 one. The four-point probe is preferred for measurement of sheet resistance (R_{sh}). Table III.7 gives R_{sh} values of the undoped and F doped SnO_2 where one can see that R_{sh} of F doped SnO_2 are relatively lower compared to the undoped SnO_2 one which means that the lowest sheet resistance has the highest electrical conductivity. High electrical conductivity is very important aspect for collecting electrode but is not sufficient condition for solar cell applications as it will be elucidate in the following subsection.

Table III.7: *Electrical parameters of SnO_2 and SnO_2: F thin films as a function of fluorine doping.*

Material	**R_{sh} (Ω)**	**Hall *N* (cm^{-3})×10^{19}**
Undoped film	138	-
SnO_2: F 3 *wt.* %	75	0.75
SnO_2: F 6 *wt.* %	21	2.04
SnO_2: F 9 *wt.* %	24	0.98
SnO_2: F 12 *wt.* %	50	0.04

The Hall Effect measurements are recapitulated in Table III.7, Hall measurements indicate that the ultrasonic sprayed SnO_2: F films have n-type semiconductors character. Figure III.17 shows that the variations of sheet resistance and free carrier concentration, as a function of fluorine concentration of SnO_2: F films, were inverted. This may be explained as follow: when fluorine is incorporated in tin oxide films, each F^- anion substitutes an O^{2-} anion in the lattice and the substituted O^{2-} anions introduce more free electrons. This results an increase in free electrons and decreases the value of R_{sh}. The decrease in the free electrons with increase in the value of R_{sh} beyond a certain doping concentration of fluorine (6-7 *wt.*% in our work) probably represents a solubility limit of fluorine in the tin oxide lattice [42]. The excess F atoms do not occupy the proper lattice positions to contribute to the free carrier concentration while, at the same time, enhance the disorder of the structure leading to an increase in sheet resistance as it was seen in the X-ray pattern for the 9 *wt.*% doped sample in Figure III.5 where more picks appeared (see section I.13 in chapter I).

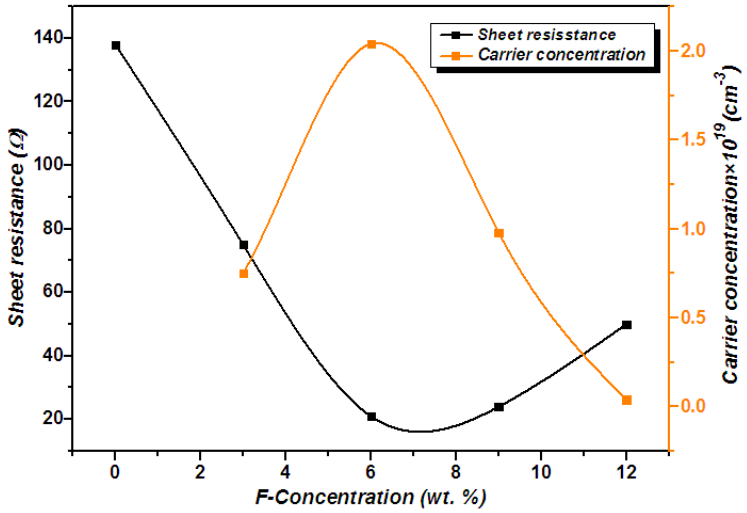

Figure III.17: *Variations of carrier concentration and sheet resistance of FTO films with different fluorine doping.*

Conclusion

In this chapter, the experimental results obtained by the analysis of the elaborated SnO_2: F thin films were introduced. The results revealed that the elaborated films are high conducting and transparent and fluorine doping enhance the quality of the films. From this chapter one can conclude the following points:

- All prepared films are polycrystalline and having SnO_2 tetragonal rutile structure;
- SEM images of the films surface shows that the substrate is well covered with fine grains and homogeneous distribution;
- For undoped SnO_2 films the average transmission, in visible region, is more than 74 % Whereas for the doped SnO_2 films, the value of transmission $T(\lambda)$, in the visible region, is located in the average 73.5–87.5 %;
- FTIR study confirmed the formation of SnO_2 with characteristic vibration modes of Sn–O and O–Sn–O, with appearing of Sn-F vibration modes after fluorine doping.
- Hall measurements indicate that the SnO_2: F films have n-type semiconductors character with carrier concentration in the average 0.04-2.04×10^{19} cm^{-3}.

The goal of this study is to determine spectroscopically the optoelectronic magnitudes of F doped SnO_2 prepared by ultrasonic spray. We had concentrated our interest on effect of fluorine doping on the structural, optical and opto-electrical properties of SnO_2 thin films.. Effect of film thickness on certain properties such as structural, optical and figure of merit has been investigated.

During this study, undoped and fluorine (0-12 *wt.* %) doped SnO_2 thin films were deposited on glass substrates by ultrasonic spray technique The prepared films have been studied and analyzed using several analyzes techniques, such as: DRX, UV-Vis, FTIR, SEM, PL, four probes and hall effect. Our results were presented and discussed broadly and we had compared our results with ones that published in the literatures, our results reveal good agreement with other researchers.

The main results obtained in the presented search may be concluding as follow:

- SnO_2 thin films were deposited, successfully, on glass substrates by ultrasonic spray method from a solution of tin chloride ($SnCl_2$) using a solvent mixed of methanol and distilled water.
- XRD characterization revealed that the undoped and F-doped SnO_2 thin films were polycrystalline with tetragonal rutile structure.
- For undoped film the crystallite size was about 24.74nm whereas it was found to decrease only, for 3 *wt.*% F doped SnO_2, to 11.58nm and increases with increasing F concentration to 28.16nm for SnO_2: F 12 *wt.* %.
- SEM images of the films surface revealed that the elaborated films having uniform morphology and the substrates were well covered.
- The prepared films have high transmittance in visible area ranging in 73.5-87.5% and transmittance values were enhanced after doping with fluorine.
- FTIR study confirmed the formation of SnO_2 with characteristic vibration modes of Sn-O and O-Sn-O, with appearing of Sn-F and F-Sn-F vibration modes after fluorine doping.
- Hall measurements indicate that the SnO_2: F films have n-type semiconductors character with carrier concentration in the average $0.04\text{-}2.04\times10^{19}cm^{-3}$.

- Obtained results demonstrate that SnO_2 thin films have good opto-electronic properties.
- Figure of merit values were calculated from sheet resistance and transmittance measurements. For fluorine effect, a maximum value of figure of merit was 9.76×10^{-3} (Ω^{-1}) at λ= 900 nm for 12 *wt.* % fluorine concentration. For thickness effect, a maximum value of figure of merit, ($13.04\times10^{-3}\Omega^{-1}$), was obtained with FTO thin films at λ= 700 nm for 440 nm thickness.
- below 7 wt.% F concentration, fluorine substitute oxygen and fill in oxygen vacancies.
- above 7 wt.% fluorine substitute oxygen, fill in oxygen vacancies and act as interstitial element in the lattice, those effects caused a decrease in carrier concentration but enhanced optical properties and figure of merit. 12 *wt.* % F doped SnO_2 reveal the highest transmittance and figure of merit values.
- Contact angle measurements confirmed that fluorine doping enhances hydrophobic properties of SnO_2 thin films. The 3 and 7 *wt.*% F doped films have the higher contact angle.

- Obtained results demonstrate the success of the ultrasonic spray technique to prepare thin films of SnO_2 with characteristics appropriate to the physical applications.
- The obtained high conducting and transparent FTO thin films are promising to be useful in various optoelectronic applications, in particular, as window layer in solar cells.

Suggestions for future:

- More detailed studies on the obtained results will take place in the future, in particular photoluminescence study.
- More extensive characterization of prepared films.
- Co-doping tin oxide will take our interest in the future.